Article

Current Biology

The conserved *iol* gene cluster in *Pseudomonas* is involved in rhizosphere competence

Highlights

- Top-tier root colonizers encode the *iol* gene cluster involved in inositol metabolism
- *iol*-deletion mutant bacteria are less competitive root colonizers
- Inositol triggers swimming through the *iol* locus and accumulation of siderophores
- The *iol* locus is conserved, expressed *in vivo*, and linked to competence

Authors

Juan J. Sánchez-Gil, Sanne W.M. Poppeliers, Jordan Vacheron, Hao Zhang, Bart Odijk, Christoph Keel, Ronnie de Jonge

Correspondence

r.dejonge@uu.nl

In brief

Sánchez-Gil et al. show that the *iol* locus in *Pseudomonas* promotes rhizosphere competitiveness. The locus enables stimulation of swimming motility and siderophore production in response to plant-derived inositol. The authors show that the locus is conserved and expressed in planta and discuss its involvement in rhizosphere competence.

Sánchez-Gil et al., 2023, Current Biology *33*, 3097–3110
August 7, 2023 © 2023 Elsevier Inc.
https://doi.org/10.1016/j.cub.2023.05.057

CellPress

Current Biology

CellPress

Article

The conserved *iol* gene cluster in *Pseudomonas* is involved in rhizosphere competence

Juan J. Sánchez-Gil,[1] Sanne W.M. Poppeliers,[1] Jordan Vacheron,[2] Hao Zhang,[1] Bart Odijk,[1] Christoph Keel,[2] and Ronnie de Jonge[1,3,4,*]

[1]Plant-Microbe Interactions, Department of Biology, Science for Life, Utrecht University, Utrecht 3584 CH, The Netherlands

[2]Department of Fundamental Microbiology, University of Lausanne, Lausanne CH-1015, Switzerland

[3]Twitter: @dejongepmi

[4]Lead contact

*Correspondence: r.dejonge@uu.nl

https://doi.org/10.1016/j.cub.2023.05.057

SUMMARY

The *Pseudomonas* genus has shown great potential as a sustainable solution to support agriculture through its plant-growth-promoting and biocontrol activities. However, their efficacy as bioinoculants is limited by unpredictable colonization in natural conditions. Our study identifies the *iol* locus, a gene cluster in *Pseudomonas* involved in inositol catabolism, as a feature enriched among superior root colonizers in natural soil. Further characterization revealed that the *iol* locus increases competitiveness, potentially caused by an observed induction of swimming motility and the production of fluorescent siderophore in response to inositol, a plant-derived compound. Public data analyses indicate that the *iol* locus is broadly conserved in the *Pseudomonas* genus and linked to diverse host-microbe interactions. Together, our findings suggest the *iol* locus as a potential target for developing more effective bioinoculants for sustainable agriculture.

INTRODUCTION

With a human population surpassing the 8 billion mark, the modern agricultural industry faces the challenge of increasing crop yields while reducing synthetic inputs. A promising solution leverages plant-beneficial microbes as soil amendments, collectively known as bioinoculants, which have shown positive effects such as promotion of plant growth, competition against phytopathogens, and activation of host immune defenses.[1] Typically, bioinoculants need to successfully colonize the rhizosphere, which comprises the roots and the region of the soil under their direct influence, to provide such benefits. Numerous candidates for bioinoculants have been identified and studied *in vitro* or in semi-controlled conditions, and the molecular mechanisms behind their positive effects are an actively studied topic. However, the natural rhizosphere environment presents significant differences that hinder the effective application of bioinoculants in agriculture. Successful colonization of the rhizosphere depends on edaphic factors (factors such as soil chemistry and structure), host genotype, and in particular, the complex web of microbial interactions in the rhizosphere microbiome that results in a strong resistance to invasion.[2] Consequently, many promising bioinoculants fail to exert their positive effects or show variable efficacy in the field. Nonetheless, many organisms commonly colonize and persist in the rhizosphere driven by their intrinsic capabilities, some reaching higher abundances than others. For example, Proteobacteria and Bacteroidetes are repeatedly found to be enriched within the rhizosphere of diverse plant species.[3] In particular, the *Pseudomonas* genus comprises many representatives of rhizosphere-competent organisms. These pseudomonads display a vast diversity of competence traits and functional plasticity that grants them the ability to inhabit the rhizosphere of many plant species, such as secretion systems, evasion of plant immune defenses, or production of antimicrobial compounds.[4–9] Characterizing the underlying genetic determinants of such rhizosphere-competent microbes can help build a mechanistic understanding of the requirements of enhanced colonization, and in turn, such information can be used to design future effective bioinoculants to be applied in the field.

With the aim of finding genetic features for rhizosphere competence in natural conditions, we here compared a set of diverse *Pseudomonas* isolates from our in-lab collection for their ability to colonize the rhizosphere and root surface of *Arabidopsis thaliana* in natural soil. Genomics analysis of the best colonizers highlighted the metabolism of *myo*-inositol (inositol), enabled by the *iol* locus, as an enriched explanatory feature for enhanced root colonization. To determine the contribution of the *iol* locus to root colonization, we generated an *iol*-deletion mutant and determined its competitiveness in root colonization assays in soil. We show that the *iol* mutant is less competitive and that, as expected, the *iol* locus is required for consumption of inositol. We further provide evidence suggesting that, besides acting as a nutrient source, inositol acts as a signal that induces swimming motility and the production of fluorescent siderophores. Genomic analyses show that the *iol* locus is broadly conserved in the *Pseudomonas* genus, and we discuss evidence of its expression and relevance in interaction with diverse hosts and successful colonization. Together, our findings suggest a relevant role for the *iol* locus and plant-derived inositol in driving rhizosphere competence in pseudomonads.

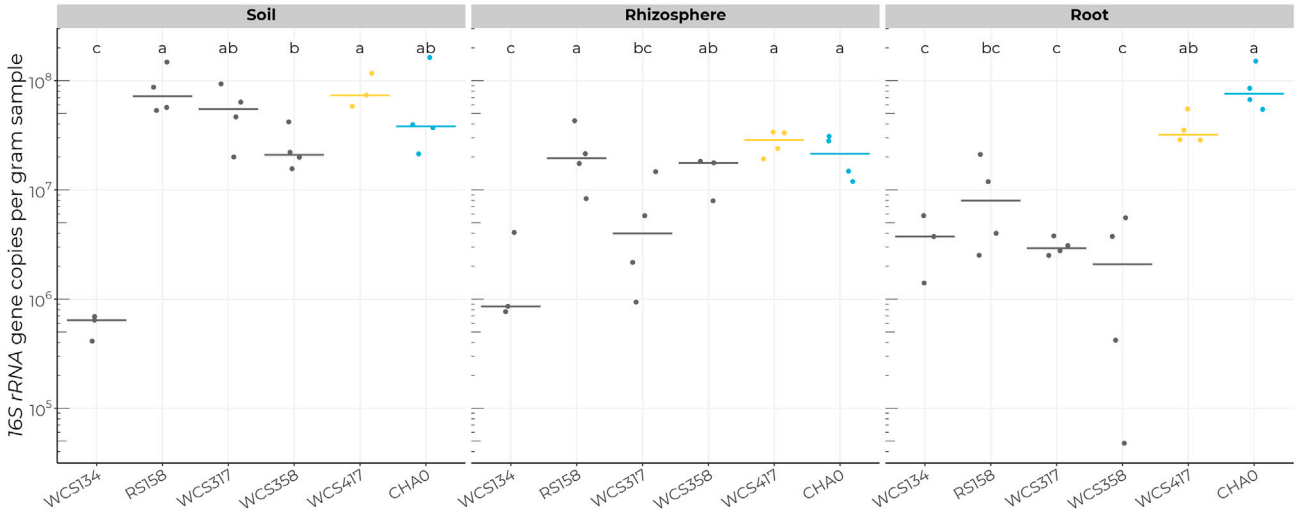

Figure 1. *P. protegens* CHA0 and *P. simiae* WCS417 are the best root colonizers

Absolute inoculum densities after 21 days post inoculation (dpi) measured as the number of *16S rRNA* copies per gram of sample found in soil (left), rhizosphere (middle), and root samples (right). The letters indicate groups of statistically different densities in each compartment according to a Sidak post hoc test on negative binomial tests. *P. protegens* CHA0 and *P. simiae* WCS417 are highlighted in cyan and yellow, respectively, to differentiate them from the remaining isolates. See also Figures S1–S3 and Table S1.

RESULTS

Competitive root colonizers are enriched for inositol phosphate metabolism

To identify genetic traits among root-associated microorganisms for competitive root colonization in natural soil conditions, we introduced a set of plant root-associated *Pseudomonas* isolates in a natural soil and subsequently compared their abundances (Figure S1). To aid in isolate selection, we sequenced and compared the genomes of a group of root-associated pseudomonads from our collection, isolated from the same natural soil, and several well-known root-associated isolates, and we chose a group of six isolates that varied in phylogenetic spectrum, source environments, and effects on host plants (Figure S2; Table S1): *Pseudomonas simiae* WCS417 (WCS417), *Pseudomonas capeferrum* WCS358 (WCS358), *Pseudomonas protegens* CHA0 (CHA0), *Pseudomonas fluorescens* RS158 (RS158), *Pseudomonas* sp. WCS317 (WCS317), and *Pseudomonas* sp. WCS134 (WCS134). We introduced these isolates individually into natural soil, reaching an inoculum density of 10^8 colony-forming units (CFUs)/g of soil, and grew *Arabidopsis thaliana* ecotype Col-0 seedlings on this soil for 21 days. Recognizing that inferences about the colonizing ability of root-associated microorganisms could be influenced by the method used to harvest the plant roots, we separated samples into two fractions: the rhizosphere, which includes soil attached to the root and that is under the influence of the root, and the rhizoplane or root fraction, which consists of the root without adhering soil. Following the extraction of these fractions, we determined the absolute abundance of each isolate in all samples by amplicon-based sequencing of the *16S rRNA* gene, using an internal control as a reference for normalization.

Isolates displayed differential population densities across fractions (Figures 1 and S3A). With the exception of WCS134, isolates survived similarly in bulk soil, although WCS358 and CHA0 showed slightly lower populations. Colonization in rhizosphere samples is in general lower than in soil, although the relative differences seen among isolates are very similar to those in soil. Root samples proved to be the most effective wash for assessing differential colonization among the isolates (Figure 1). Specifically, WCS417 and CHA0 exhibited approximately 8.6- and 20-fold higher colonization levels, respectively, compared with the rest of the isolates. We expected each isolate to show intermediate abundances in the rhizosphere fraction compared with soil and roots. However, CHA0 and WCS134 reached higher populations in root than in rhizosphere samples; WCS417 colonizes the rhizosphere and root fractions equally; and RS158, WCS317, and WCS358 exhibit higher abundances in the rhizosphere fraction, which suggests differing lifestyles among these pseudomonads (Figure S3B).

Based on these results, we selected WCS417 and CHA0 as the best root colonizers and proceeded to investigate the genetic traits underlying their superior root colonization.

To investigate the genetic traits that distinguish these organisms from others, we extracted the orthologous protein families shared by WCS417 and CHAO. In total, we identified 203 such families exclusively found in the best colonizers (Figure 2A), comprising 204 and 206 orthologs in WCS417 and CHA0, respectively. Biosynthesis of antibiotics and biofilm formation were the most common annotations in these genes, accounting for approximately 5% of the orthologs each (12 genes in WCS417 and 10 genes in CHA0 for biosynthesis of antibiotics, and 10 genes in each microbe for biofilm formation). Notably, enrichment analysis on the annotations identified metabolism of inositol phosphate, the fourth most common annotation, as the most enriched function, followed by the tenth most common annotation for biosynthesis of siderophores (Figure 2B). The strong enrichment for inositol phosphate metabolism is caused by the presence of a locus (hereafter *iol* locus) in WCS417 and CHA0 that is absent in the other isolates (Figure 2C). The locus

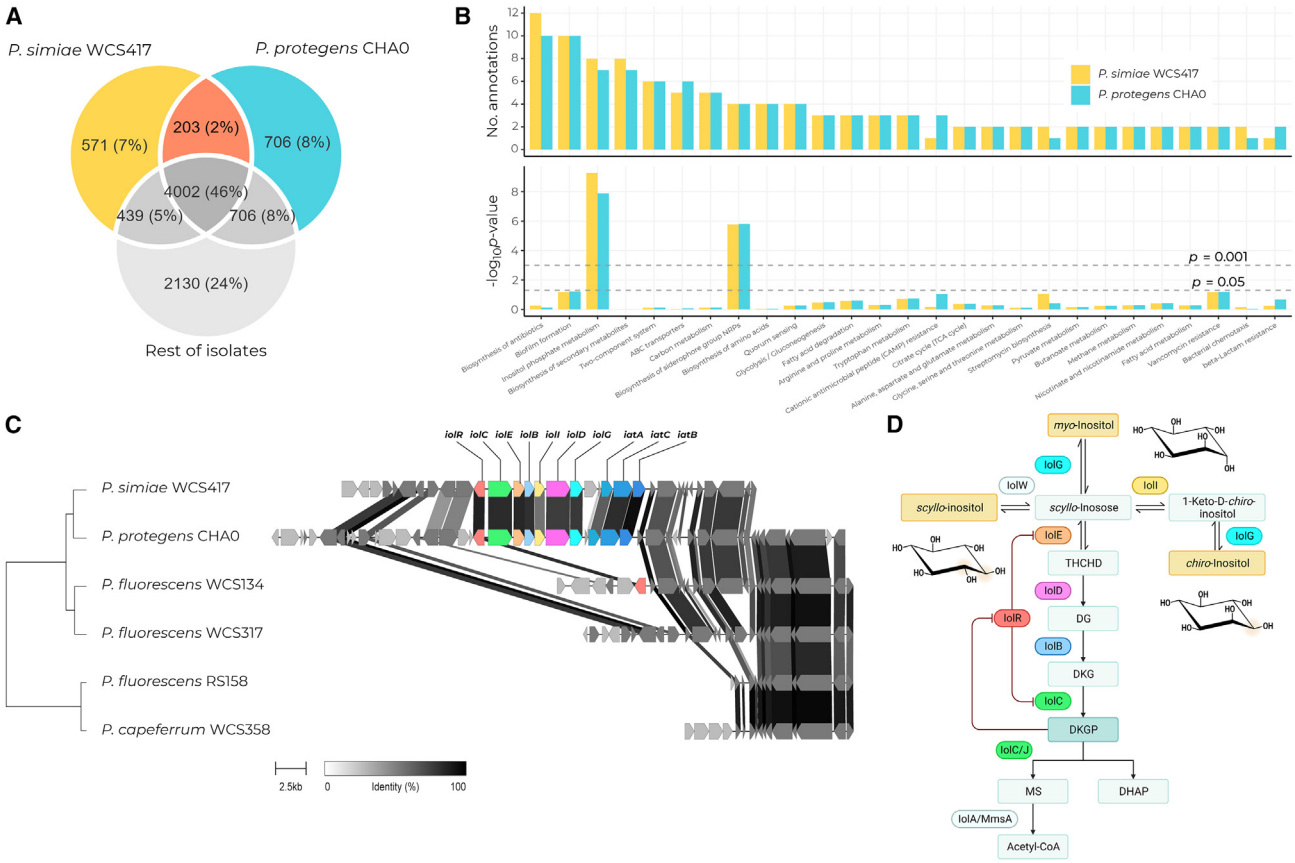

Figure 2. Inositol phosphate metabolism is the most enriched function in the best root colonizers

(A) Venn diagram depicting the genetic relationships between the best root colonizers and the rest of the isolates. The orange area shows the set of orthologous protein families present in the genomes of WCS417 and CHA0 but absent in the other pseudomonads.

(B) Bar plots showing the counts for KEGG pathway annotations (left) and their FDR-adjusted p value in a Fisher's enrichment test for the set of shared orthologs between WCS417 and CHA0, versus the other pseudomonads in this study. Only the annotations that are found more than once are shown. Note that the most enriched function is inositol phosphate metabolism.

(C) Phylogenetic tree of the isolates in this study and the *iol* locus responsible for the enrichment in the annotations for inositol phosphate metabolism.

(D) Predicted pathway for inositol metabolism in *Pseudomonas*. The proteins in the pathway are colored as the genes in (C). The chiral positions (C1, C2) that distinguish the *myo*, *scyllo*, and *chiro* enantiomers of inositol are shown as a shaded area on the 3D structural representations.

THCHD, 3,5/4-trihydroxycyclohexa-1,2-dione; DG, 5-deoxy-glucuronate; DKG, 2-deoxy-5-keto-D-gluconate; DKGP, 2-deoxy-5-keto-D-gluconate-6-phosphate; MS, malonic semialdehyde (3-oxopropanoate); DHAP, dihydroxyacetone phosphate. Pathway in (D) was created with BioRender.com.

spans 14 and 13 kbp in WCS417 and CHA0, respectively, and comprises 10 genes: a transcription factor (*iolR*), six genes responsible for inositol catabolism (*iolCEBIDG*), and three genes that encode an ABC transporter responsible for inositol intake (*iatABC*). In WCS417, an extra gene, *mocA*, encoding an oxidoreductase, is located upstream of the ABC transporters.

The IolCEBIDG enzymes potentially catalyze five consecutive reactions that transform the sugar alcohol *myo*-inositol successively into *scyllo*-inosose (IolG), trihydroxycyclohexadione (IolE), deoxyglucuronate (IolD), deoxy-keto-glucuronate (IolB), deoxy-keto-gluconate-6-phosphate (DKGP; IolC), and malonate semialdehyde and dihydroxyacetone phosphate (DHAP; IolC) (Figure 2D), which could theoretically enter other pathways or be directed toward anabolism as acetyl-coenzyme A (CoA) in a reaction catalyzed by MmsA/IolA, which is codified elsewhere in both pseudomonad genomes. The predicted transcriptional repressor of the locus, IolR, is inhibited by the interaction with the intermediate product DKGP, allowing the expression of the entire locus.[10–12]

The *iol* locus enhances competence in natural soil

To investigate the contribution of the *iol* locus to pseudomonad competence in soil, we created the multi-gene Δ*iolRCEBIDG* mutant (Δ*iol*) in CHA0 and subsequently assessed its plant root colonization. We inoculated GFP-tagged CHA0 wild-type (WT) cells and mCherry-tagged Δ*iol* mutant cells individually and a 1:1 mixture of both genotypes in soil as before, reaching an inoculum density of 10^8 CFU/g of soil, and then grew *Arabidopsis* seedlings for 21 days on this soil. In individual inoculations, the colonization ability of both genotypes in soil and on the plant root was equivalent (Figure 3A). However, when co-inoculated, WT cells dramatically outcompeted mutant cells, achieving a 5.3-fold higher median density on the roots (Figure 3B). Interestingly, although the mutant achieves

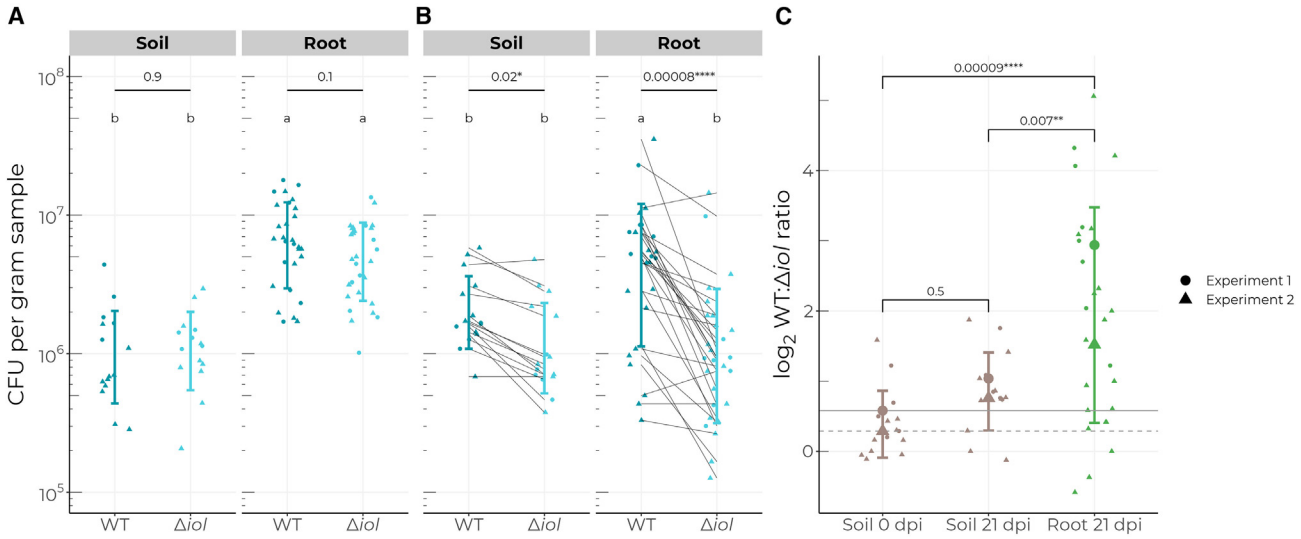

Figure 3. The *iol* locus enhances root colonizing competence in *P. protegens* CHA0

(A) CFU counts per gram of sample of WT and mutant cells in individual inoculations in soil (left) and root samples (right) at 21 dpi. Significance values derive from a negative binomial test for count data, adjusting for variations between experiments.

(B) Paired CFU counts of each genotype in the mixed 1:1 co-inoculation at 21 dpi in soil (left) and roots (right). Significance is calculated using a paired t test on all pair-wise comparisons.

The letters in (A) and (B) indicate groupings according to a negative binomial model adjusted for experimental variation. Notice that the number of Δ*iol* cells in co-inoculation experiments is similar on roots and in soil.

(C) Log_2-transformed ratio of WT and Δ*iol* mutant cells in the mixed treatment. Large shapes indicate the median ratio per experiment, whereas lines show the mean initial ratio per experiment (solid line: experiment 1; dashed line: experiment 2). On the roots, WT cells achieve a significantly higher population at 21 dpi, reaching an approximate ratio of 5:1.

comparable densities when inoculated individually, its density on the root in competition was the same as in soil, suggesting that the root was primarily colonized by WT cells. As expected, the WT:Δ*iol* ratio on the root indicates a clear plant-driven advantage of WT cells (Figure 3C).

The *iol* locus is required for catabolism of inositol

To confirm the contribution of the *iol* locus to inositol catabolism, we performed growth curve measurements using inositol as the sole carbon source in minimal M9 medium. Our results showed that Δ*iol* mutant cells did not exhibit any growth after 80 h, in contrast to WT cells, which could utilize inositol to grow, albeit to only half the density reached with glucose (Figures 4A and 4B).

In non-minimal CC medium supplemented with inositol, we observed a comparable growth curve dynamic in WT cells after 36 h (Figures 4C and 4D), although the growth benefit was transient and variable (Figure S4). Surprisingly, we observed that inositol induced a decline in the density of Δ*iol* mutant cells after the exponential phase, at around 12 h, suggesting that inositol may have a toxic or bacteriostatic effect on these cells.

Inositol enhances swimming motility through the *iol* locus

Inositol metabolism has been linked to motility and other relevant root colonization traits in previous studies.[13–16] Based on this, we hypothesized that the enhanced competitiveness of CHA0 in soil may also be due to an induction of motility by inositol. To test this hypothesis, we conducted typical bacterial swimming and swarming assays as we did previously for spontaneous root-competitive *P. protegens* CHA0 mutants[17] in the absence and presence of inositol. These experiments revealed that inositol improved swimming motility of WT cells by 30% after 48 h, whereas it decreased swimming ability of mutant cells by 30% (Figure 5). Intriguingly, we observed that, although WT cell swarming motility is unaffected by the addition of inositol, mutant cell swarming is totally abolished in this condition (Figure S5). Glucose supplementation only promoted swimming at a 10-fold higher concentration, although the mean radius was still 10% smaller than that observed with inositol. This finding, together with the reduced growth benefit of inositol, suggests that inositol likely functions as a signal in addition to, or rather than, that of an advantageous carbon source.

Besides the effect on swimming, we noticed that mutant colonies exhibited a fainter color, analogous to the decrease in optical density during planktonic growth at the onset of the stationary phase in growth curve assays. Therefore, we decided to monitor the changes in its phenotype over time in a dedicated assay. Here, we performed multiple inoculations again in swimming plates, inoculating both genotypes either individually or in combination. Mutant cells growing with inositol were visibly similar to the WT at 1 day post inoculation (dpi), but the color intensity of the colonies faded after reaching the end of the plate, approximately at the end of the second day (Figure S6). Intriguingly, we observed scattered mutant colonies reappearing in plates with inositol at 6 dpi, but only in plates where the mutants grew individually (Figure 6A). Moreover, WT colonies at this time

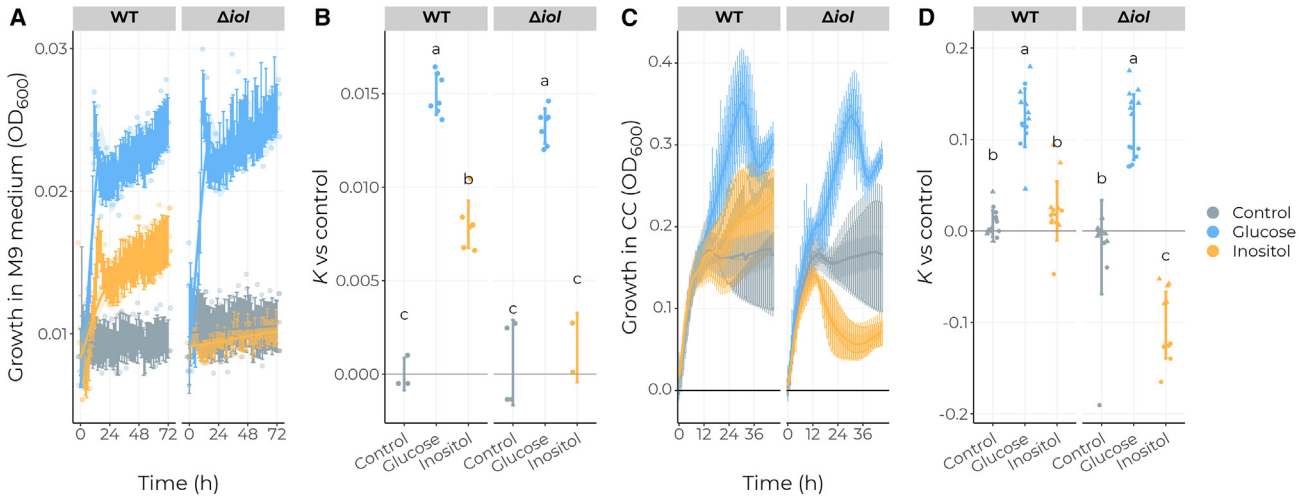

Figure 4. The *iol* locus is required for using inositol as a sole carbon source and affects the growth of Δ*iol* cells on inositol

(A) Growth curves of WT and Δ*iol* mutant cell populations in non-supplemented minimal M9 medium (control) or in M9 medium supplemented with 100 mM glucose or inositol measured as OD at 600 nm. Mutant cells are unable to grow with inositol, indicating that the *iol* locus is required to catabolize inositol.

(B) Fitted maximum population size (carrying capacity, *K*) of the growth data in (A).

(C) Growth curves in non-supplemented CC medium (control) or in CC medium supplemented with 10 mM glucose or inositol. The data summarize two independent growth curve assays. Despite the variability within treatments across experiments, the curves show that both genotypes stabilize in the stationary phase in control medium. Mutant cells growing in inositol-supplemented medium follow a similar pattern during the stationary phase (0–12 h), but then the optical density drops noticeably.

(D) Fitted carrying capacity (*K*, maximum population size) of the growth data in (C).

For both assays, every time point consists of measurements for seven technical replicates.

See also Figure S4.

exhibited visibly brighter yellow colonies, indicative of an increased production of fluorescent siderophores (Figure 6). Altogether, these results suggest a role for the *iol* locus and inositol metabolism in quorum behavior and competence in the rhizosphere.

The *iol* locus is broadly conserved among pseudomonads and a determinant for diverse host-microbe interactions

Considering the potential of the *iol* locus in determining the competitiveness of pseudomonads in the rhizosphere, we hypothesized that it would be a conserved trait in the *Pseudomonas* genus (Figure 7). Exploratory analysis of all 15,742 *Pseudomonas* genomes in the NCBI RefSeq database revealed that the *iol* locus is found in the majority of *Pseudomonas* species. The most notable exception is *Pseudomonas aeruginosa*, none of which encoded the *iol* locus (8,781 genomes, ~56% of all genomes). From the remaining 6,962 genomes, approximately 67% contain six or more *iol* genes spaced less than 20 kbp from each other or distributed over a limited number of genomic loci, yielding a total of 4,642 *iol*+ pseudomonads. Genomes in which the *iol* genes could not be found in a single locus typically had a low assembly quality (N50 < 50 kbp) and were considered *iol*+ if they met the requirement of the minimum number of six genes in a small (2–3) number of loci. In general, *pseudomonads* exhibit a binary *iol* locus presence-absence distribution at the species level. The frequency of *iol*+ strains is over 90% in 11 out of 23 species and over 80% in 14 out of 23 species, not including the umbrella species *Pseudomonas fluorescens* and *Pseudomonas* spp. The remaining nine species contain at most 10% (*Pseudomonas koreensis*) *iol*+ representatives (Figure 7B).

Among *iol*+ genomes, the core *iolRCEBDG* genes are found in a very high frequency, between 97% and 100% of genomes, indicative of co-evolution as a locus and suggesting that all genes are required to perform their biological function in the proposed catabolic pathway. Interestingly, around 10% of *iol*+ genomes lack *iolI* (454 pseudomonads), and the distribution of these 454 over the phylogenetic tree suggests that *iolI* loss occurred multiple times throughout the evolution of the genus. *iolI* encodes an inosose isomerase, which is responsible for the conversion of 1-keto-D-*chiro*-inositol into *scyllo*-inosose. The absence of *iolI* could therefore indicate the lack of *chiro*-inositol-derived compounds in the environment of these specific organisms. Other common structures of the locus contain a copy of a methylmalonate semialdehyde dehydrogenase (*iolA/mmsA*) between *iolB* and *iolD* and/or a sugar phosphate isomerase/epimerase between *iolG* and the *iatACB* genes, potentially *iolH* (Figure 7C). Neither of these genes was found in WCS417 or CHA0. Last, a gene encoding a transcription factor, *dksA*, and a putative chemotaxis protein, *mcp*, are located downstream of the *iatACB* genes, suggesting a direct connection between the *iol* locus and motility.

In order to search for more evidence of the relationship between root colonization and the *iol* locus, we explored publicly available transposon-insertion sequencing (Tn-seq) data in WCS417.[19] In this study, a collection of random insertion WCS417 mutants was let to colonize *Arabidopsis* roots in plates for seven days, after which the abundance of each

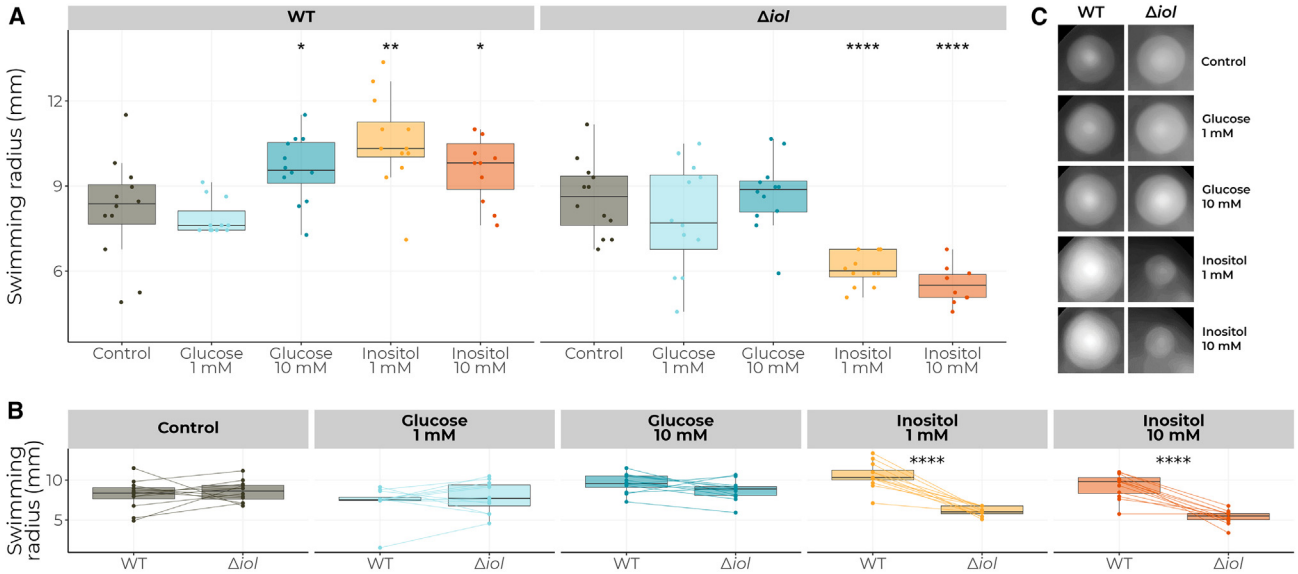

Figure 5. Inositol enhances swimming motility through the *iol* locus in *P. protegens* CHA0

(A) Swimming radius of WT (left) and Δ*iol* mutant cells (right) in CC medium either unsupplemented or supplemented with glucose or inositol at 1 or 10 mM. Inositol induces swimming motility at 1 mM in WT cells, whereas motility is suppressed in the mutant.

(B) Same data as in (A) but shown per treatment and pairing the swimming halo for both genotypes per plate, highlighting the genotype-dependent differences in motility.

(C) Representative images of WT and Δ*iol* mutant cell swimming behavior in each treatment.

See also Figure S5.

mutant was used to assign a fitness (or performance) value for root colonization for each gene. According to our analysis, root colonization appears to be supported by *iolR*, the *iatABC* transporters, *iolD*, and the *traR/dksA* transcription activator. However, the remaining genes in the locus (*iolCEBIG*) did not show a significant contribution to colonization, suggesting that consumption of inositol is not per se the most determinant feature for successful colonization *in vitro* (Figure 7D). To further investigate the relationship between inositol and colonization in the context of the *iol* locus, we made use of publicly available data from additional genome-wide, transposon mutant-based fitness experiments in WCS417, in which mutants were exposed to many different conditions, including stresses, carbon and nitrogen sources, and motility assays.[20] We used these data to construct a bipartite network connecting the genes in the *iol* locus to the conditions where they showed a significant fitness contribution (Figure 7E). Unexpectedly, although most of the genes seemed related to the metabolism of inositol, neither *iolR* nor *dksA* appear to contribute directly to fitness in inositol as a sole carbon source. Instead, our analysis revealed that *iolR* is primarily related to consumption of other carbohydrates, whereas *dksA* plays a role in survival when cultured with antimicrobial compounds. Both transcription factors contribute to susceptibility to stressors such as nitrate, choline, and imidazolium chloride and promote survival in gentamicin. Interestingly, we observed a negative relationship between *dksA* and swimming motility, suggesting that the induction of motility by inositol in WT cells might be due to an inositol-induced inhibition of DksA activity. We did not find any obvious connection to the production of fluorescent siderophores.

Based on the manifest connection between root colonization and the locus, we set out to explore its expression during host colonization. For this, we examined publicly available data from a study performed by Vesga et al.[21] Here, the transcriptional activity of *P. protegens* CHA0 was assayed during the colonization of the hemolymph of an insect host (*Galleria mellonella*), of the insect gut (*Plutella xylostella*), and of wheat roots (*Triticum aestivum*).[21] We found that the *iol* locus is expressed during colonization on wheat roots and in the insect gut, but not in the insect hemolymph. Considering that hemolymph data were collected following direct injection, these data suggest that the *iol* locus is related to host perception and/or colonization (Figure 7F).

DISCUSSION

In our study, we compared the colonization ability of a set of pseudomonads in non-sterile natural soil by amplicon-based sequencing of the *16S rRNA* gene. The use of spike-in internal controls for absolute quantification from complex environments has been applied in recent studies[22,23] and permits high-throughput quantification that does not depend on isolate-specific resistance markers and/or dilution series of the samples. Using this approach, we found that the compared colonization ability in our set of isolates varied substantially between rhizosphere and root samples (Figure 1), which suggests that these pseudomonads exhibit different lifestyles and environmental preferences: microbes enriched on the root will be firmly attached to the host and embedded in a biofilm on the surface, i.e., WCS417 and CHA0, whereas organisms preferring the rhizosphere might benefit from diffusing nutrients and potentially

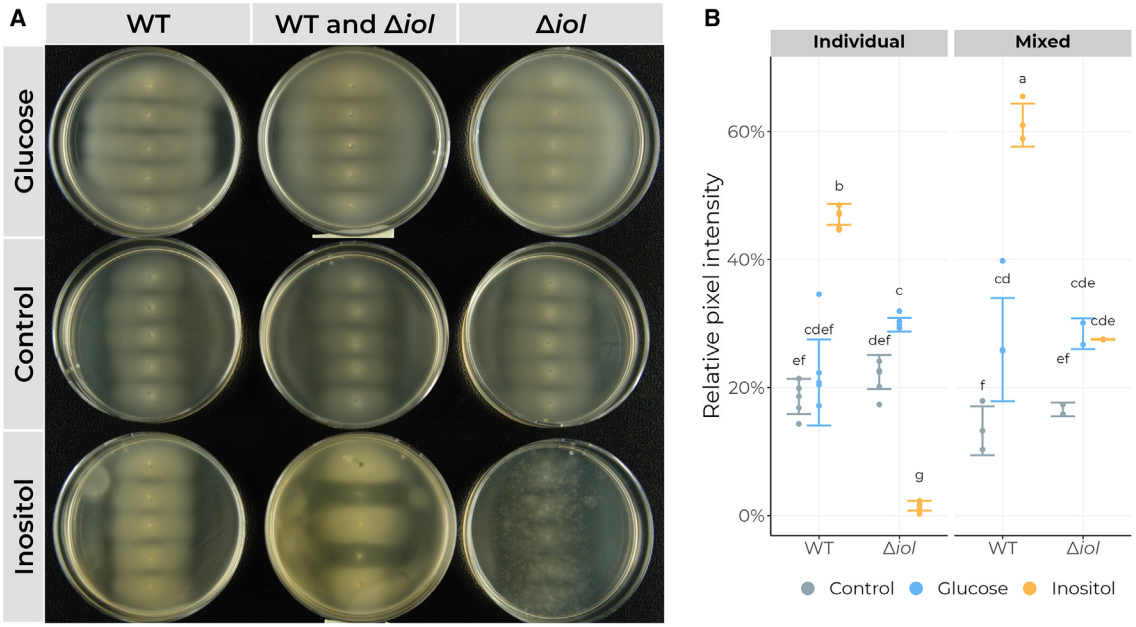

Figure 6. Inositol enhances the production of fluorescent siderophores and affects Δ*iol* mutant physiology. Qualitative assessment of the effect of inositol and glucose on WT and Δ*iol* mutant cells

(A) Representative images of colonies at 6 dpi in swimming plates supplemented with 10 mM glucose (first row), unsupplemented (second row), or supplemented with 10 mM inositol (third row). The first and third columns show 5 inoculations of WT and mutant cells, respectively. The second column shows a combined inoculation of mutant cells surrounded by WT cells, used to evaluate possible interactions between both genotypes. Note how WT colonies show a brighter yellow color, characteristic of fluorescent siderophore production. Mutant colonies disintegrate at 3 dpi, and colonies re-appear at 6 dpi as seemingly independent and scattered populations.

(B) Qualitative measurement of siderophores produced in the plates shown in (A) using the intensity of yellow pixels as a proxy.

See also Figure S6.

avoid stress from an active immune system. In any case, our findings indicate that careful consideration of method selection should be taken in microbial colonization studies because different treatments might select for microbes with different lifestyles and lead to disparate conclusions about their ecological competence.

The two best root colonizers, WCS417 and CHA0, are well-known pseudomonads that have been widely studied for their plant-beneficial effects.[7,24,25] The adaptation to a plant-associated lifestyle requires optimized consumption of plant-derived resources, among which inositol and its derivatives play an important role. In plants, inositol polyphosphates are main constituents of the plasma membrane and have key roles in signaling, immunity, and phosphorus storage,[26–29] and inositol exudation through root tissues has been reported in many species.[30,31] In fact, the ability to metabolize inositol emerged as a potentially distinctive trait in plant-associated pseudomonads in a genomic meta-analysis,[32] supporting the idea that the presence of the *iol* locus in WCS417 and CHA0 arises, indeed, from optimized adaptation to plant hosts. In general, expression of the *iol* genes *in planta* or in response to root exudates has also been observed in previous studies, although often indirectly or outside of the experimental focus. Expression of the *iol* genes in isolates from the genera *Cupriavidus*, *Burkholderia*, and *Rhizobium* was upregulated in response to root exudates of the legume *Mimosa pudica*.[33] In pseudomonads, expression of the locus and its relation to competence have also been observed in isolates with divergent lifestyles. The pathogen *Pseudomonas syringae* pv. *tomato* DC3000 expresses the *iol* genes when grown in tomato apoplast extracts[34] and during growth in the *Arabidopsis* apoplast.[35] Likewise, *Pseudomonas syringae* pv. *syringae* B728a requires a functional *iol* locus for full pathogenicity in bean leaves (*Phaseolus vulgaris*), especially during apoplastic colonization.[36,37] Notably, we found that the vast majority of *Pseudomonas syringae* genomes are *iol*+, highlighting its relevance for this plant pathogenic bacterium (Figure 7B). These findings are further corroborated by a recent comprehensive analysis of the distribution of the *iol* locus by Weber and Fuchs.[38] Their analysis revealed that hundreds of bacteria from diverse families and disparate ecological niches encode the capacity to catabolize inositol via the *iol* locus. These include animal and plant pathogens, soil commensals, and rhizosphere-associated bacteria similar to the pseudomonads discussed here.[38]

However, the precise physiological function of the *iol* locus seems to be variable and isolate specific. In a study comparing the expression patterns of a selection of eight pseudomonads in response to root exudates from *Brachypodium distachyon*, six out of eight strains showed upregulation of *iol* genes.[39] *Pseudomonas protegens* Pf-5, the closest relative of CHA0, increased the expression of the entire locus and yet did not exhibit any growth when grown in inositol as a sole carbon source, suggesting again that utilization of inositol for growth

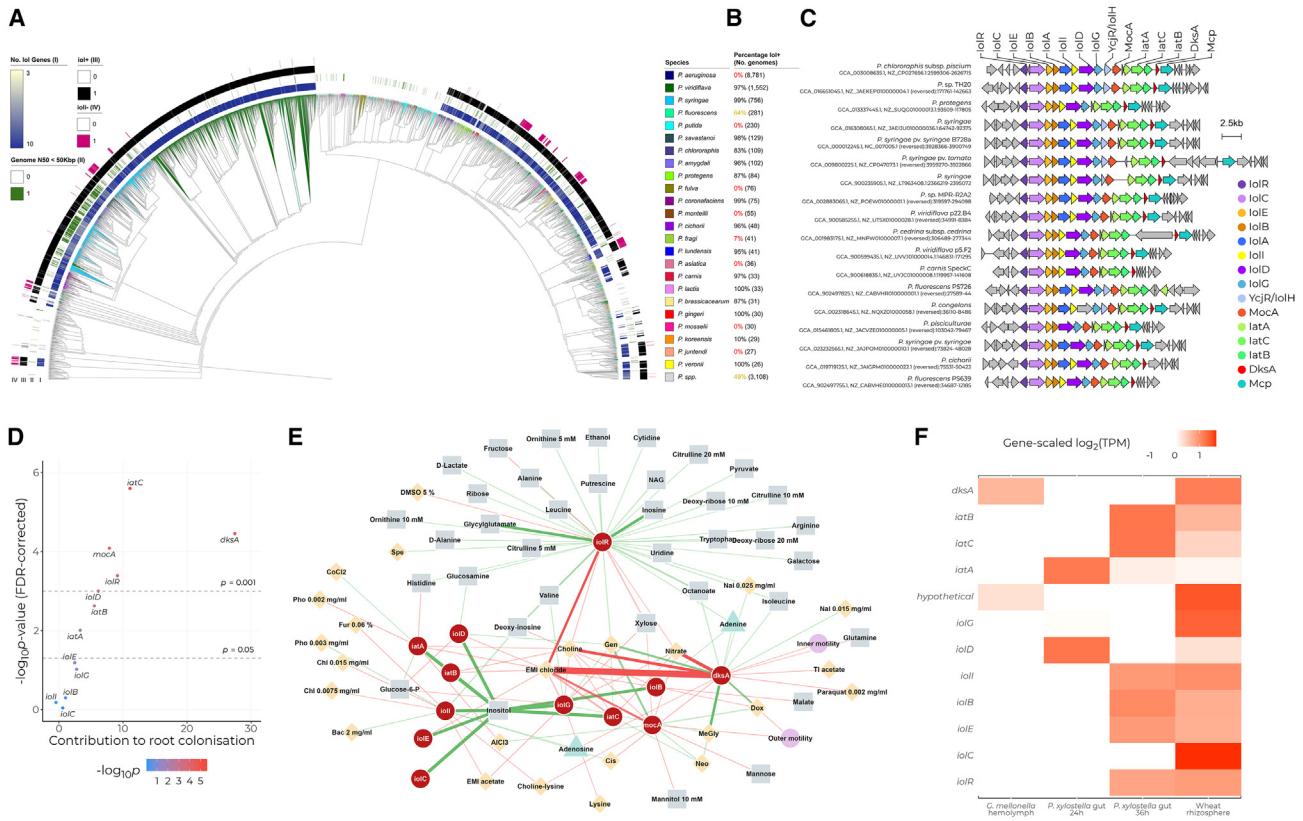

Figure 7. The *iol* locus is conserved in the *Pseudomonas* genus and contributes to diverse host-microbe interactions

(A) Phylogenetic tree of 15,743 *Pseudomonas* genomes available in the NCBI RefSeq database showing the distribution of the *iol* locus in the genus. 8,781 *P. aeruginosa* genomes, evolutionary distinct from the other 6,962 *Pseudomonas* genomes and all lacking the *iol* locus, were pruned from the tree. Ring I: number of *iol* genes in the highest scoring locus on the respective genome based on cblaster.[18] Ring II: factor indicating whether the N50 value ($\log_2$ scaled) for a given genome is below 50 kbp as a measure for genome assembly integrity. Ring III: summary of all significantly *iol*+-scoring regions throughout the genome (minimal 6 out of 10 genes), confirming that genomes with fewer *iol* genes in the best scoring locus (ring I, light-colored) typically have a low genome N50 (ring II, green) but still encode the full locus. Ring IV: factor indicating the absence of *iolI* in the locus, showing that the loss of *iolI* follows a non-phylogenetic pattern in the genus.

(B) Summary of the frequency of *iol*+ genomes in each *Pseudomonas* species, according to the annotated species names.

(C) Locus alignment from a representative set of genomes in the tree, showing locus conservation in the genus. Some loci harbor an extra *iol* gene, *iolA/mmsA*, downstream of *iolB*, and two other genes, *mocA* and *ycjR*, encoding the sugar phosphate isomerase/epimerase *iolH*, upstream of the genes encoding the ABC transporters.

(D) Scatterplot showing the relative contribution of the genes in the *iol* locus in *P. simiae* WCS417 to *Arabidopsis* root colonization *in vitro* based on publicly available mutant fitness data.[19] The x axis represents the contribution of each gene to colonization, using the *t*-like effect-size statistic versus initial mutant populations, as previously reported.[19] The y axis represents the FDR-corrected p value for the contribution of each gene, as inverse logarithm of the raw value for ease of interpretation.

(E) Bipartite network depicting the contribution of each gene in the *iol* locus in *P. simiae* WCS417 to survival in different environments included in the Fitness Browser.[20] Genes are shown as red nodes, and links connect these with conditions in which they show differential fitness across genome-wide fitness assays. Green and red links indicate a positive or negative contribution to survival, respectively. Link width and opacity indicate link weight (absolute contribution). Conditions are colored by their nature: carbon sources (gray), stressors (yellow), or nitrogen sources (light teal). Notice how *iolR* is not directly related to survival in inositol but in a myriad of other carbon sources and specific stressors. Notably, *iol* genes show many links to antimicrobial compounds. EMI, ethylmethylimidazolium; Gen, gentamicin; Neo, neomycin; Pho, phosphomycin; Dox, doxycycline; BAC, bacitracin; Chl, chloramphenicol; Cis, cisplatin; Fur, furfuraldehyde; Nal, nalidixate; Spe, spectinomycin; DMSO, dimethylsulfoxide; CoCl2, cobalt (II) chloride; AlCl3, aluminium (III) chloride; Tl acetate, thallium acetate; MeGly, methylglyoxal.

(F) Heatmap of gene expression data from Vesga et al.,[21] showing expression of the *P. protegens* CHA0 *iol* locus during insect and plant colonization/infection. Other relevant colonization genes are also included. Expression data are shown as gene-scaled $\log_2$-scaled transcripts per million).

is not the only function of the locus. In fact, upregulation of the *iol* locus in the other pseudomonads in their study, either fully or partially, did not seem to be a requirement for growth in inositol at all.

In our root colonization assays, Δ*iol* mutant CHA0 cells can colonize equally with WT cells when inoculated individually, whereas in competition with WT cells, they fail to reach a higher population density than in soil. We also observed growth defects in mutant cells when grown in inositol. Interestingly, a similar phenomenon has been described in the Alphaproteobacteria *Sinorhizobium meliloti*, *Sinorhizobium fredii*, and *Rhizobium leguminosarum*, where the *iol* genes play an important role in defining competence in root nodules.[13] In *Sinorhizobium*, *iolG* mutants form abnormal bacteroids,

are impaired in nitrogen fixation, and are unable to utilize rhizopines, *scyllo*-inositol derivatives produced in nodules, which ultimately results in a loss of competitiveness against WT cells.[15,40–42] Yet these growth defects do not seem to pose a disadvantage in our individual inoculations because mutant density on the root is not different from WT populations. The stimulation of swimming motility in WT cells by inositol, however, might promote quicker arrival during initial stages of colonization and therefore enable an earlier occupation of the root surface. In fact, expression of the *iol* genes is restricted to the initial phase of infection in the plant pathogen *Ralstonia solanacearum* via a quorum-sensing mechanism. Moreover, knockout mutants for *iolG* in this pathogen are impaired in their capacity to colonize tomato roots during the initial stages of infection,[14] and remarkably, swimming motility during this phase has also been linked to successful pathogenicity in an independent study.[43] A direct link between inositol and bacterial motility was previously observed in *Priestia megaterium* (formerly *Bacillus megaterium*). In this organism, inositol exuded by the roots of Arabidopsis and tomato plants (*Solanum lycopersicum*) induced a strong chemotactic response and enhanced biofilm formation.[16] Noteworthy, quorum-dependent responses, such as the one described in *Ralstonia* and *Priestia*, commonly take place in the transition to the stationary phase.[44] Furthermore, rhizopines, which act as quorum-sensing signals in *Sinorhizobium* species,[45] affect motility, growth, and biofilm formation and also act during the stationary phase and not before.[46] The connection between inositol metabolism, the *iol* locus, and quorum behavior could explain the decrease in optical density in the Δ*iol* CHA0 at the onset of the stationary phase that we observe and, additionally, the enhanced production of siderophores that we observed after 6 days on plates. This is further supported by our results in swarming motility, for which quorum-based coordination is required,[47,48] where inositol does not seem to affect swarming of WT cells, whereas it abolishes swarming in the *iol* mutant.

Our findings imply an important role for the *iol* locus during *Pseudomonas* root colonization beyond the utilization of inositol as a carbon source. Our analyses of publicly available genome-wide fitness data show that root colonization *in vitro* depends primarily on the *iolR*, *iatABC*, and *dksA* genes while being seemingly independent of inositol consumption. Additionally, IolR does not affect inositol consumption, contrasting with previous results,[10–12] but is required for root colonization and exhibits many links to the metabolism of diverse carbon sources. Moreover, swimming motility appears to be inhibited by DksA, suggesting that the induction of swimming by inositol in our experiments might be due to an inositol-induced repression of DksA. Together with our findings on the overproduction of fluorescent siderophores, this information supports a more complex mechanism in response to the presence of host-derived inositol in the environment. Indeed, IolR regulates behavioral responses toward inositol in other organisms, such as the expression of type III secretion system in *Salmonella typhimurium*,[49] xylose uptake in *Corynebacterium glutamicum*,[50] or cell autoaggregation and biofilm formation in *Aeromonas hydrophila*.[10] Interestingly, cell aggregation by the Pel and Psl exopolysaccharides (EPS) increases siderophore production in *Pseudomonas aeruginosa* by raising internal levels of cyclic di-GMP, which, in turn, triggers a Gac-mediated activation of genes related to siderophores production.[51] At the same time, survival in the stationary phase and the production of Pel and Psl EPS are enabled by the sigma factor RpoS.[52] It seems, therefore, plausible to hypothesize that our observed increase in production of fluorescent siderophores in WT cells is due to an interaction with RpoS in the stationary phase, resulting in an inositol-induced change in EPS composition and an eventual increase in siderophore production. This would translate into enhanced iron-scavenging capabilities in WT cells in response to host clues, with host-derived inositol as a proxy, whereas in mutant cells, a misregulation of RpoS activity could be the cause of aberrant growth in the stationary phase.

In general, the *iol* locus has been associated with a myriad of different phenotypes in other bacteria, and its physiological and ecological functions also seem to go beyond the mere obtention of energy from inositol. Instead, the locus appears to be embedded in a complex mechanism of sensing and responding to host-related environmental cues. For example, in *Caulobacter crescentus*, the iron-deficiency response regulator Fur represses expression of the *iol* locus in an iron-independent manner,[53] and in *Salmonella typhimurium*, the locus is linked to antibiotic resistance.[54] In salmonellae, the small RNA *RssR* controls expression of the *iol* locus and inositol metabolism,[55] leading to complex expression dynamics controlled at the bacterial population level.[56]

The specificity of the phenotype associated with the *iol* locus in pseudomonads may be reflected in the diversity of locus decorations. Our analysis of the *iol* locus among available *Pseudomonas* genomes shows that, besides the core locus (*iolR-CEBDG*), specific conformations with additional genes can be found. In particular, we observed that *iolI* has been lost in ∼10% of *iol*+ pseudomonads. The inosose isomerase IolI enables the uptake of *chiro*-inositol through the conversion of 1-keto-D-*chiro*-inositol into *scyllo*-inosose, which can be readily incorporated into the main pathway. Although derivatives of inositol can be found in soil in diverging amounts, the *chiro* conformation is rare in soil. However, it is produced by plants of many species in differing amounts and forms,[28,57–59] which further supports the link between the presence of *iolI* and a plant-associated lifestyle. Together with the lack of well-defined taxon-specific loss of *iolI*, this suggests that the different structures of the *iol* locus that we described here might correspond to host-specific locus conformations according to the composition of host exudates. Divergent *iol* loci in *Pseudomonas* can include several other genes, such as *iolA*, *mocA*, and *dksA*. The methylmalonate semialdehyde dehydrogenase IolA/MmsA produces acetyl-CoA from the last digestion product in the predicted pathway, malonate semialdehyde, or malonyl-CoA from methylmalonate semialdehyde. This gene is frequently found elsewhere in the genome, suggesting that this conversion can be regulated in both inositol-dependent and -independent ways. The *mocA* gene was originally annotated as a Gfo/Idh/MocA-like oxidoreductase, which is a large protein family with many disparate functions described, among them the metabolism of rhizopines in *Sinorhizobium* species.[60] In parallel, annotations of this gene in some pseudomonads suggest that

this gene might encode a homolog of IolW, a *scyllo*-inositol dehydrogenase that catalyzes the conversion of this inositol enantiomer into *scyllo*-inosose and allows its incorporation in the main pathway. Both annotations, MocA and IolW, point toward the use of *scyllo*-inositol or rhizopine derivatives and possible associations with nodulating bacteria. Further experiments are required to clarify whether pseudomonads can in fact use rhizopines or other *scyllo*-inositol-derived or -exuded compounds in the rhizosphere. Last, DksA, encoded in the 3′ end of the locus, appears involved in survival in stress induced by methylglyoxal in our analysis of the publicly available genome-wide fitness data. This is one of the few reported phenotypes for IolS in *Bacillus* species, an aldo-keto reductase with an otherwise unknown function.[61,62] Similar to DksA in pseudomonads, IolS does not seem to be required for inositol metabolism, yet it is conserved in the *iol* locus in bacilli and upregulated in response to maize exudates.[63]

In conclusion, we show that the *iol* locus determines rhizosphere competence in pseudomonads. Detailed characterization further revealed that its function entails more complex mechanisms than mere consumption of the sugar alcohol *myo*-inositol and that these mechanisms are taxon and, possibly, host specific. In parallel with our study, O'Banion et al.[64] also identified inositol as an important plant-derived compound determining root colonization phenotypes in *Pantoea*, including an enhancement of bacterial motility among them. In our pseudomonad, plant-derived inositol might induce the repression of DksA and enable an enhancement of swimming motility, subsequently promoting early arrival in the rhizosphere, prompter colonization, and therefore enhanced competitiveness. However, the aberrant growth in mutant cells during the switch to the stationary phase implies an additional mechanism during this phase that results in increased capability of iron scavenging of WT cells. Future research should dig deeper into the mechanistic processes by which competence is optimized by the *iol* locus in the *Pseudomonas* genus, including the potential role of RpoS and EPS production and composition. The findings in our study provide evidence of the fundamental basis of rhizosphere colonization and signify an important step toward the development of robust bioinoculants in sustainable agriculture.

STAR★METHODS

Detailed methods are provided in the online version of this paper and include the following:

- KEY RESOURCES TABLE
- RESOURCE AVAILABILITY
  - Lead contact
  - Materials availability
  - Data and code availability
- EXPERIMENTAL MODEL AND SUBJECT DETAILS
  - Arabidopsis thaliana
  - Bacterial cultures
- METHOD DETAILS
  - Soil treatments, transplantations, and microbiome sampling
  - DNA extractions, *16S rRNA* amplicon library preparation, and data normalization
  - Genomic analysis
  - Mutant construction
  - Root colonization and competition assays
  - Growth assays
  - Motility assays and siderophore plates
  - Analyses on publicly available data
- QUANTIFICATION AND STATISTICAL ANALYSIS

SUPPLEMENTAL INFORMATION

Supplemental information can be found online at https://doi.org/10.1016/j.cub.2023.05.057.

ACKNOWLEDGMENTS

The authors want to thank Bas E. Dutilh, Corné M.J. Pieterse, and members of the Plant-Microbe Interactions lab for helpful discussions. We acknowledge the Utrecht Sequencing Facility (USEQ) for providing sequencing service and data. USEQ is subsidized by the University Medical Center Utrecht and the Netherlands X-omics Initiative (NWO project 184.034.019). This study was supported by the NWO Green II grant no. ALWGR.2017.002 (S.W.M.P., J.J.S.-G., and R.d.J.), the Novo Nordisk Foundation grant no. NNF19SA0059362 (R.d.J.), and the China Scholarship Council scholarship no. 201406300090 (H.Z.).

AUTHOR CONTRIBUTIONS

Conceptualization, J.J.S.-G.; methodology, J.J.S.-G., J.V., C.K., and H.Z.; software, J.J.S.-G.; validation, J.J.S.-G. and R.d.J.; formal analysis, J.J.S.-G. and R.d.J.; investigation, J.J.S.-G., S.W.M.P., and B.O.; resources, J.V., C.K., and H.Z.; data curation, J.J.S.-G.; writing – original draft, J.J.S.-G.; writing – review & editing, J.V., C.K., and R.d.J.; supervision, R.d.J.; project administration, R.d.J.; funding acquisition, R.d.J.

DECLARATION OF INTERESTS

The authors declare no competing interests.

Received: March 24, 2023
Revised: April 25, 2023
Accepted: May 24, 2023
Published: July 6, 2023

REFERENCES

1. Bakker, P.A.H.M., Berendsen, R.L., Van Pelt, J.A., Vismans, G., Yu, K., Li, E., Van Bentum, S., Poppeliers, S.W.M., Sanchez Gil, J.J., Zhang, H., et al. (2020). The soil-borne identity and microbiome-assisted agriculture: looking back to the future. Mol. Plant *13*, 1394–1401. https://doi.org/10.1016/j.molp.2020.09.017.
2. Poppeliers, S.W., Sánchez-Gil, J.J., and de Jonge, R. (2023). Microbes to support plant health: understanding bioinoculant success in complex conditions. Curr. Opin. Microbiol. *73*, 102286. https://doi.org/10.1016/j.mib.2023.102286.
3. Ling, N., Wang, T., and Kuzyakov, Y. (2022). Rhizosphere bacteriome structure and functions. Nat. Commun. *13*, 836. https://doi.org/10.1038/s41467-022-28448-9.
4. Bernal, P., Allsopp, L.P., Filloux, A., and Llamas, M.A. (2017). The *Pseudomonas putida* T6SS is a plant warden against phytopathogens. ISME J. *11*, 972–987. https://doi.org/10.1038/ismej.2016.169.
5. Liu, Z., Beskrovnaya, P., Melnyk, R.A., Hossain, S.S., Khorasani, S., O'Sullivan, L.R., Wiesmann, C.L., Bush, J., Richard, J.D., and Haney, C.H. (2018). A genome-wide screen identifies genes in

rhizosphere-associated *Pseudomonas* required to evade plant defenses. mBio *9*, e00433-18, https://doi.org/10.1128/mBio.00433-18.

6. Passarelli-Araujo, H., Franco, G.R., and Venancio, T.M. (2022). Network analysis of ten thousand genomes shed light on *Pseudomonas* diversity and classification. Microbiol. Res. *254*, 126919. https://doi.org/10.1016/j.micres.2021.126919.
7. Pieterse, C.M.J., Berendsen, R.L., de Jonge, R., Stringlis, I.A., Van Dijken, A.J.H., Van Pelt, J.A.H., Van Wees, S.C.M., Yu, K., Zamioudis, C., and Bakker, P.A.H.M. (2021). *Pseudomonas simiae* WCS417: star track of a model beneficial rhizobacterium. Plant Soil *461*, 245–263. https://doi.org/10.1007/s11104-020-04786-9.
8. Yu, K., Liu, Y., Tichelaar, R., Savant, N., Lagendijk, E., van Kuijk, S.J.L., Stringlis, I.A., van Dijken, A.J.H., Pieterse, C.M.J., Bakker, P.A.H.M., et al. (2019). Rhizosphere-associated *Pseudomonas* suppress local root immune responses by gluconic acid-mediated lowering of environmental pH. Curr. Biol. *29*, 3913–3920.e4. https://doi.org/10.1016/j.cub.2019.09.015.
9. Zboralski, A., and Filion, M. (2020). Genetic factors involved in rhizosphere colonization by phytobeneficial *Pseudomonas* spp. Comp. Struct. Biotechnol. J. *18*, 3539–3554. https://doi.org/10.1016/j.csbj.2020.11.025.
10. Dong, Y., Li, S., Zhao, D., Liu, J., Ma, S., Geng, J., Lu, C., and Liu, Y. (2020). IolR, a negative regulator of the *myo*-inositol metabolic pathway, inhibits cell autoaggregation and biofilm formation by downregulating RpmA in *Aeromonas hydrophila*. npj Biofilms Microbiomes *6*, 22. https://doi.org/10.1038/s41522-020-0132-3.
11. Hellinckx, J., Heermann, R., Felsl, A., and Fuchs, T.M. (2017). High binding affinity of repressor IolR avoids costs of untimely induction of *myo*-inositol utilization by *Salmonella typhimurium*. Sci. Rep. *7*, 44362. https://doi.org/10.1038/srep44362.
12. Kohler, P.R.A., Choong, E.-L., and Rossbach, S. (2011). The RpiR-like repressor IolR regulates inositol catabolism in *Sinorhizobium meliloti*. J. Bacteriol. *193*, 5155–5163. https://doi.org/10.1128/JB.05371-11.
13. Fry, J., Wood, M., and Poole, P.S. (2001). Investigation of *myo*-inositol catabolism in *Rhizobium leguminosarum* bv. *viciae* and its effect on nodulation competitiveness. Mol. Plant Microbe Interact. *14*, 1016–1025. https://doi.org/10.1094/MPMI.2001.14.8.1016.
14. Hamilton, C.D., Steidl, O.R., MacIntyre, A.M., Hendrich, C.G., and Allen, C. (2021). *Ralstonia solanacearum* depends on catabolism of *myo*-inositol, sucrose, and trehalose for virulence in an infection stage-dependent manner. Mol. Plant Microbe Interact. *34*, 669–679. https://doi.org/10.1094/MPMI-10-20-0298-R.
15. Kohler, P.R.A., Zheng, J.Y., Schoffers, E., and Rossbach, S. (2010). Inositol catabolism, a key pathway in *Sinorhizobium meliloti* for competitive host nodulation. Appl. Environ. Microbiol. *76*, 7972–7980. https://doi.org/10.1128/AEM.01972-10.
16. Vílchez, J.I., Yang, Y., He, D., Zi, H., Peng, L., Lv, S., Kaushal, R., Wang, W., Huang, W., Liu, R., et al. (2020). DNA demethylases are required for *myo*-inositol-mediated mutualism between plants and beneficial rhizobacteria. Nat. Plants *6*, 983–995. https://doi.org/10.1038/s41477-020-0707-2.
17. Li, E., Zhang, H., Jiang, H., Pieterse, C.M.J., Jousset, A., Bakker, P.A.H.M., and de Jonge, R. (2021). Experimental-evolution-driven identification of *Arabidopsis* rhizosphere competence genes in *Pseudomonas protegens*. mBio *12*, e0092721, https://doi.org/10.1128/mBio.00927-21.
18. Gilchrist, C.L.M., Booth, T.J., van Wersch, B., van Grieken, L., Medema, M.H., and Chooi, Y.-H. (2021). cblaster: a remote search tool for rapid identification and visualization of homologous gene clusters. Bioinform. Adv. *1*, vbab016. https://doi.org/10.1093/bioadv/vbab016.
19. Cole, B.J., Feltcher, M.E., Waters, R.J., Wetmore, K.M., Mucyn, T.S., Ryan, E.M., Wang, G., Ul-Hasan, S., McDonald, M., Yoshikuni, Y., et al. (2017). Genome-wide identification of bacterial plant colonization genes. PLoS Biol. *15*, e2002860, https://doi.org/10.1371/journal.pbio.2002860.
20. Price, M.N., Wetmore, K.M., Waters, R.J., Callaghan, M., Ray, J., Liu, H., Kuehl, J.V., Melnyk, R.A., Lamson, J.S., Suh, Y., et al. (2018). Mutant phenotypes for thousands of bacterial genes of unknown function. Nature *557*, 503–509. https://doi.org/10.1038/s41586-018-0124-0.
21. Vesga, P., Flury, P., Vacheron, J., Keel, C., Croll, D., and Maurhofer, M. (2020). Transcriptome plasticity underlying plant root colonization and insect invasion by *Pseudomonas protegens*. ISME J. *14*, 2766–2782. https://doi.org/10.1038/s41396-020-0729-9.
22. Kim, J.Y., Yi, M.-H., Kim, M., Lee, S., Moon, H.S., Yong, D., and Yong, T.-S. (2021). Measuring the absolute abundance of the microbiome by adding yeast containing 16S rRNA gene from a hyperthermophile. Microbiologyopen *10*, e1220, https://doi.org/10.1002/mbo3.1220.
23. Tkacz, A., Hortala, M., and Poole, P.S. (2018). Absolute quantitation of microbiota abundance in environmental samples. Microbiome *6*, 110. https://doi.org/10.1186/s40168-018-0491-7.
24. Haas, D., and Défago, G. (2005). Biological control of soil-borne pathogens by fluorescent pseudomonads. Nat. Rev. Microbiol. *3*, 307–319. https://doi.org/10.1038/nrmicro1129.
25. Kupferschmied, P., Maurhofer, M., and Keel, C. (2013). Promise for plant pest control: root-associated pseudomonads with insecticidal activities. Front. Plant Sci. *4*, 287. https://doi.org/10.3389/fpls.2013.00287.
26. Castrillo, G., Teixeira, P.J.P.L., Paredes, S.H., Law, T.F., de Lorenzo, L., Feltcher, M.E., Finkel, O.M., Breakfield, N.W., Mieczkowski, P., Jones, C.D., et al. (2017). Root microbiota drive direct integration of phosphate stress and immunity. Nature *543*, 513–518. https://doi.org/10.1038/nature21417.
27. Dindas, J., DeFalco, T.A., Yu, G., Zhang, L., David, P., Bjornson, M., Thibaud, M.-C., Custódio, V., Castrillo, G., Nussaume, L., et al. (2022). Direct inhibition of phosphate transport by immune signaling in Arabidopsis. Curr. Biol. *32*, 488–495.e5. https://doi.org/10.1016/j.cub.2021.11.063.
28. Gomes, C.I., Obendorf, R.L., and Horbowicz, M. (2005). *myo*-inositol, D-*chiro*-inositol, and D-pinitol synthesis, transport, and galactoside formation in soybean explants. Crop Sci. *45*, 1312–1319. https://doi.org/10.2135/cropsci2004.0247.
29. Tan, X., Calderon-Villalobos, L.I.A., Sharon, M., Zheng, C., Robinson, C.V., Estelle, M., and Zheng, N. (2007). Mechanism of auxin perception by the TIR1 ubiquitin ligase. Nature *446*, 640–645. https://doi.org/10.1038/nature05731.
30. Chaparro, J.M., Badri, D.V., and Vivanco, J.M. (2014). Rhizosphere microbiome assemblage is affected by plant development. ISME J. *8*, 790–803. https://doi.org/10.1038/ismej.2013.196.
31. Pini, F., East, A.K., Appia-Ayme, C., Tomek, J., Karunakaran, R., Mendoza-Suárez, M., Edwards, A., Terpolilli, J.J., Roworth, J., Downie, J.A., et al. (2017). Bacterial biosensors for *in vivo* spatiotemporal mapping of root secretion. Plant Physiol. *174*, 1289–1306. https://doi.org/10.1104/pp.16.01302.
32. Levy, A., Salas Gonzalez, I., Mittelviefhaus, M., Clingenpeel, S., Herrera Paredes, S., Miao, J., Wang, K., Devescovi, G., Stillman, K., Monteiro, F., et al. (2017). Genomic features of bacterial adaptation to plants. Nat. Genet. *50*, 138–150. https://doi.org/10.1038/s41588-017-0012-9.
33. Klonowska, A., Melkonian, R., Miché, L., Tisseyre, P., and Moulin, L. (2018). Transcriptomic profiling of *Burkholderia phymatum* STM815, *Cupriavidus taiwanensis* LMG19424 and *Rhizobium mesoamericanum* STM3625 in response to *Mimosa pudica* root exudates illuminates the molecular basis of their nodulation competitiveness and symbiotic evolutionary history. BMC Genomics *19*, 105. https://doi.org/10.1186/s12864-018-4487-2.
34. Rico, A., and Preston, G.M. (2008). *Pseudomonas syringae* pv. *tomato* DC3000 uses constitutive and apoplast-induced nutrient assimilation pathways to catabolize nutrients that are abundant in the tomato apoplast. Mol. Plant Microbe Interact. *21*, 269–282. https://doi.org/10.1094/MPMI-21-2-0269.

35. Nobori, T., Velásquez, A.C., Wu, J., Kvitko, B.H., Kremer, J.M., Wang, Y., He, S.Y., and Tsuda, K. (2018). Transcriptome landscape of a bacterial pathogen under plant immunity. Proc. Natl. Acad. Sci. USA *115*, E3055–E3064. https://doi.org/10.1073/pnas.1800529115.

36. Helmann, T.C., Deutschbauer, A.M., and Lindow, S.E. (2019). Genome-wide identification of *Pseudomonas syringae* genes required for fitness during colonization of the leaf surface and apoplast. Proc. Natl. Acad. Sci. USA *116*, 18900–18910. https://doi.org/10.1073/pnas.1908858116.

37. Yu, X., Lund, S.P., Scott, R.A., Greenwald, J.W., Records, A.H., Nettleton, D., Lindow, S.E., Gross, D.C., and Beattie, G.A. (2013). Transcriptional responses of *Pseudomonas syringae* to growth in epiphytic versus apoplastic leaf sites. Proc. Natl. Acad. Sci. USA *110*, E425–E434. https://doi.org/10.1073/pnas.1221892110.

38. Weber, M., and Fuchs, T.M. (2022). Metabolism in the niche: a large-scale genome-based survey reveals inositol utilization to be widespread among soil, commensal, and pathogenic bacteria. Microbiol. Spectr. *10*, e0201322. https://doi.org/10.1128/spectrum.02013-22.

39. Mavrodi, O.V., McWilliams, J.R., Peter, J.O., Berim, A., Hassan, K.A., Elbourne, L.D.H., LeTourneau, M.K., Gang, D.R., Paulsen, I.T., Weller, D.M., et al. (2021). Root exudates alter the expression of diverse metabolic, transport, regulatory, and stress response genes in rhizosphere *Pseudomonas*. Front. Microbiol. *12*, 651282. https://doi.org/10.3389/fmicb.2021.651282.

40. Galbraith, M.P., Feng, S.F., Borneman, J., Triplett, E.W., de Bruijn, F.J., and Rossbachl, S. (1998). A functional *myo*-inositol catabolism pathway is essential for rhizopine utilization by *Sinorhizobium meliloti*. Microbiology (Reading) *144*, 2915–2924. https://doi.org/10.1099/00221287-144-10-2915.

41. Jiang, G., Krishnan, A.H., Kim, Y.W., Wacek, T.J., and Krishnan, H.B. (2001). A functional *myo*-inositol dehydrogenase gene is required for efficient nitrogen fixation and competitiveness of *Sinorhizobium fredii* USDA191 to nodulate soybean (*Glycine max* [L.] Merr.). J. Bacteriol. *183*, 2595–2604. https://doi.org/10.1128/JB.183.8.2595-2604.2001.

42. Murphy, P.J., Wexler, W., Grzemski, W., Rao, J.P., and Gordon, D. (1995). Rhizopines—their role in symbiosis and competition. Soil Biol. Biochem. *27*, 525–529. https://doi.org/10.1016/0038-0717(95)98627-Z.

43. Corral, J., Sebastià, P., Coll, N.S., Barbé, J., Aranda, J., and Valls, M. (2020). Twitching and swimming motility play a role in *Ralstonia solanacearum* pathogenicity. mSphere *5*, e00740-19, https://doi.org/10.1128/mSphere.00740-19.

44. Goo, E., Majerczyk, C.D., An, J.H., Chandler, J.R., Seo, Y.-S., Ham, H., Lim, J.Y., Kim, H., Lee, B., Jang, M.S., et al. (2012). Bacterial quorum sensing, cooperativity, and anticipation of stationary-phase stress. Proc. Natl. Acad. Sci. USA *109*, 19775–19780. https://doi.org/10.1073/pnas.1218092109.

45. Zuniga-Soto, E., Fitzpatrick, D.A., Doohan, F.M., and Mullins, E. (2019). Insights into the transcriptomic response of the plant engineering bacterium *Ensifer adhaerens* OV14 during transformation. Sci. Rep. *9*, 10344. https://doi.org/10.1038/s41598-019-44648-8.

46. Krysciak, D., Grote, J., Rodriguez Orbegoso, M., Utpatel, C., Förstner, K.U., Li, L., Schmeisser, C., Krishnan, H.B., and Streit, W.R. (2014). RNA sequencing analysis of the broad-host-range strain *Sinorhizobium fredii* NGR234 identifies a large set of genes linked to quorum sensing-dependent regulation in the background of a *traI* and *ngrI* deletion mutant. Appl. Environ. Microbiol. *80*, 5655–5671. https://doi.org/10.1128/AEM.01835-14.

47. Akbari Kiarood, S.L., Rahnama, K., Golmohammadi, M., and Nasrollanejad, S. (2020). Quorum-quenching endophytic bacteria inhibit disease caused by *Pseudomonas syringae* pv. syringae in *Citrus* cultivars. J. Basic Microbiol. *60*, 746–757. https://doi.org/10.1002/jobm.202000038.

48. Daniels, R., Vanderleyden, J., and Michiels, J. (2004). Quorum sensing and swarming migration in bacteria. FEMS Microbiol. Rev. *28*, 261–289. https://doi.org/10.1016/j.femsre.2003.09.004.

49. Cordero-Alba, M., Bernal-Bayard, J., and Ramos-Morales, F. (2012). SrfJ, a *Salmonella* type III secretion system effector regulated by PhoP, RcsB, and IolR. J. Bacteriol. *194*, 4226–4236. https://doi.org/10.1128/JB.00173-12.

50. Klaffl, S., Brocker, M., Kalinowski, J., Eikmanns, B.J., and Bott, M. (2013). Complex regulation of the phosphoenolpyruvate carboxykinase gene *pck* and characterization of its GntR-type regulator IolR as a repressor of *myo*-inositol utilization genes in *Corynebacterium glutamicum*. J. Bacteriol. *195*, 4283–4296. https://doi.org/10.1128/JB.00265-13.

51. Visaggio, D., Pasqua, M., Bonchi, C., Kaever, V., Visca, P., and Imperi, F. (2015). Cell aggregation promotes pyoverdine-dependent iron uptake and virulence in *Pseudomonas aeruginosa*. Front. Microbiol. *6*, 902. https://doi.org/10.3389/fmicb.2015.00902.

52. Irie, Y., Starkey, M., Edwards, A.N., Wozniak, D.J., Romeo, T., and Parsek, M.R. (2010). *Pseudomonas aeruginosa* biofilm matrix polysaccharide Psl is regulated transcriptionally by RpoS and post-transcriptionally by RsmA. Mol. Microbiol. *78*, 158–172. https://doi.org/10.1111/j.1365-2958.2010.07320.x.

53. da Silva Neto, J.F., Lourenço, R.F., and Marques, M.V. (2013). Global transcriptional response of *Caulobacter crescentus* to iron availability. BMC Genomics *14*, 549. https://doi.org/10.1186/1471-2164-14-549.

54. Lynch, J.A., and Kierstead, M.E. (1985). Antibiotic resistance associated with inositol metabolism in salmonellae from Ontario cattle. Can. Vet. J. *26*, 251–253.

55. Kröger, C., Rothhardt, J.E., Brokatzky, D., Felsl, A., Kary, S.C., Heermann, R., and Fuchs, T.M. (2018). The small RNA RssR regulates *myo*-inositol degradation by *Salmonella enterica*. Sci. Rep. *8*, 17739. https://doi.org/10.1038/s41598-018-35784-8.

56. Kröger, C., Srikumar, S., Ellwart, J., and Fuchs, T.M. (2011). Bistability in *myo*-inositol utilization by *Salmonella enterica* serovar Typhimurium. J. Bacteriol. *193*, 1427–1435. https://doi.org/10.1128/JB.00043-10.

57. Siracusa, L., Napoli, E., and Ruberto, G. (2022). Novel chemical and biological insights of inositol derivatives in Mediterranean plants. Molecules *27*, 1525. https://doi.org/10.3390/molecules27051525.

58. Turner, B.L., Papházy, M.J., Haygarth, P.M., and Mckelvie, I.D. (2002). Inositol phosphates in the environment. Philos. Trans. R. Soc. Lond. B Biol. Sci. *357*, 449–469. https://doi.org/10.1098/rstb.2001.0837.

59. Xia, T., and Wang, Q. (2006). D-*chiro*-inositol found in *Cucurbita ficifolia* (Cucurbitaceae) fruit extracts plays the hypoglycaemic role in streptozocin-diabetic rats. J. Pharm. Pharmacol. *58*, 1527–1532. https://doi.org/10.1211/jpp.58.10.0014.

60. Taberman, H., Parkkinen, T., and Rouvinen, J. (2016). Structural and functional features of the NAD(P) dependent Gfo/Idh/MocA protein family oxidoreductases. Protein Sci. *25*, 778–786. https://doi.org/10.1002/pro.2877.

61. Chandrangsu, P., Dusi, R., Hamilton, C.J., and Helmann, J.D. (2014). Methylglyoxal resistance in *Bacillus subtilis*: contributions of bacillithiol-dependent and independent pathways. Mol. Microbiol. *91*, 706–715. https://doi.org/10.1111/mmi.12489.

62. Ehrensberger, A.H., and Wilson, D.K. (2004). Structural and catalytic diversity in the two family 11 aldo-keto reductases. J. Mol. Biol. *337*, 661–673. https://doi.org/10.1016/j.jmb.2004.01.059.

63. Fan, B., Carvalhais, L.C., Becker, A., Fedoseyenko, D., von Wirén, N., and Borriss, R. (2012). Transcriptomic profiling of *Bacillus amyloliquefaciens* FZB42 in response to maize root exudates. BMC Microbiol. *12*, 116. https://doi.org/10.1186/1471-2180-12-116.

64. O'Banion, B.S., Jones, P., Demetros, A.A., Kelley, B.R., Wagner, A.S., Chen, J.-G., Muchero, W., Reynolds, T.B., Jacobson, D., and Lebeis, S.L. (2023). Plant inositol transport influences bacterial colonization phenotypes. Preprint at bioRxiv. https://doi.org/10.1101/2023.05.03.538913.

65. Martínez-García, E., and de Lorenzo, V. (2011). Engineering multiple genomic deletions in Gram-negative bacteria: analysis of the multi-resistant antibiotic profile of *Pseudomonas putida* KT2440. Environ. Microbiol. *13*, 2702–2716. https://doi.org/10.1111/j.1462-2920.2011.02538.x.

66. R Core Team (2019). R: A Language and Environment for Statistical Computing (R Foundation for Statistical Computing). https://www.R-project.org/.

67. Wickham, H. (2016). ggplot2: Elegant Graphics for Data Analysis, Second Edition (Springer International Publishing).

68. Kassambara, A. (2020). ggpubr: 'ggplot2' based publication ready plots. The Comprehensive R Archive Network. https://cran.r-project.org/web/packages/ggpubr/index.html.

69. Gao, C.-H. (2022). ggVennDiagram: a 'ggplot2' implement of Venn diagram. The Comprehensive R Archive Network. https://cran.r-project.org/web/packages/ggVennDiagram/ggVennDiagram.pdf.

70. Tenenbaum, D.; Bioconductor Package Maintainer (2022). KEGGREST: client-side REST access to the Kyoto Encyclopedia of Genes and Genomes (KEGG). https://bioconductor.org/packages/release/bioc/html/KEGGREST.html.

71. Callahan, B.J., McMurdie, P.J., Rosen, M.J., Han, A.W., Johnson, A.J.A., and Holmes, S.P. (2016). DADA2: high-resolution sample inference from Illumina amplicon data. Nat. Methods *13*, 581–583. https://doi.org/10.1038/nmeth.3869.

72. Hothorn, T., Bretz, F., and Westfall, P. (2008). Simultaneous inference in general parametric models. Biom. J. *50*, 346–363. https://doi.org/10.1002/bimj.200810425.

73. Wickham, H., François, R., Henry, L., and Müller, K. (2022). dplyr: a grammar of data manipulation. https://dplyr.tidyverse.org/.

74. Venables, W.N., and Ripley, B.D. (2002). Modern Applied Statistics with S, Fourth Edition (Springer). https://doi.org/10.1007/978-0-387-21706-2.

75. Lenth, R.V. (2023). emmeans: estimated marginal means, aka least-squares means. The Comprehensive R Archive Network. https://cran.r-project.org/web/packages/emmeans/emmeans.pdf.

76. Bache, S., and Wickham, H. (2022). magrittr: a forward-pipe operator for R. The Comprehensive R Archive Network. https://cran.r-project.org/web/packages/magrittr/magrittr.pdf.

77. Wilke, C.O., and Wiernik, B.M. (2022). ggtext: improved text rendering support for 'ggplot2'. The Comprehensive R Archive Network. https://cran.r-project.org/web/packages/ggtext/readme/README.htmlhttps://cran.r-project.org/web/packages/ggtext/readme/README.html.

78. Pedersen, T.L. (2022). patchwork: the composer of plots. The Comprehensive R Archive Network. https://patchwork.data-imaginist.com/reference/patchwork-package.html.

79. Xiao, N. (2018). ggsciggsci: scientific journal and sci-fi themed color palettes for 'ggplot2'. The Comprehensive R Archive Network.

80. Briatte, F. (2023). ggnet2: network visualization with ggplot2. https://briatte.github.io/ggnet/.

81. Butts, C.T. (2008). Network: a package for managing relational data in R. J. Stat. Softw. *24*, 1–36. https://doi.org/10.18637/jss.v024.i02.

82. Sprouffske, K., and Wagner, A. (2016). Growthcurver: an R package for obtaining interpretable metrics from microbial growth curves. BMC Bioinformatics *17*, 172. https://doi.org/10.1186/s12859-016-1016-7.

83. Harrell, F.E., Jr. (2022). Hmisc: Harrell miscellaneous. The Comprehensive R Archive Network. https://cran.r-project.org/web/packages/Hmisc/index.html.

84. Kolde, R. (2019). Pheatmap: Pretty heatmaps. R package version 1.0.12.. The Comprehensive R Archive Network https://CRAN.R-project.org/package=pheatmap.

85. Wickham, H., and Seidel, D. (2022). Scales: scale functions for visualization. The Comprehensive R Archive Network. https://scales.r-lib.org/.

86. Chang, W. (2023). Extrafont: tools for using fonts. The Comprehensive R Archive Network. https://cran.r-project.org/web/packages/extrafont/index.html.

87. Wickham, H. (2019). Assertthat: easy pre and post assertions. The Comprehensive R Archive Network. https://cran.r-project.org/web/packages/assertthat/index.html.

88. Pagès, H., Aboyoun, P., Gentleman, R., and DebRoy, S. (2023). Biostrings: efficient manipulation of biological strings. Bioconductor. https://doi.org/10.18129/B9.bioc.Biostrings.

89. Peterson, B.G., and Carl, P. (2020). PerformanceAnalytics: econometric tools for performance and risk analysis. The Comprehensive R Archive Network. https://cran.r-project.org/web/packages/PerformanceAnalytics/index.html.

90. Wickham, H.; RStudio (2022). stringr: simple, consistent wrappers for common string operations. The Comprehensive R Archive Network. https://cran.r-project.org/web/packages/stringr/index.html.

91. Ooms, J. (2021). magick: advanced graphics and image-processing in R. The Comprehensive R Archive Network. https://cran.r-project.org/web/packages/magick/vignettes/intro.html.

92. Wickham, H., and Bryan, J. (2022). readxl: read Excel files. The Comprehensive R Archive Network. https://cran.r-project.org/web/packages/readxl/index.html.

93. Slowikowski, K. (2022). ggrepel: automatically position non-overlapping text labels with 'ggplot2'.. The Comprehensive R Archive Network https://rdrr.io/cran/ggrepel/#:~:text=Labels%20with%20'ggplot2'-,ggrepel%3A%20Automatically%20Position%20Non%2DOverlapping%20Text%20Labels%20with%20'ggplot2,away%20from%20the%20data%20points.

94. Wickham, H., Vaughan, D., and Girlich, M. (2023). tidyr: tidy messy data. The Comprehensive R Archive Network. https://cran.r-project.org/web/packages/tidyr/index.html.

95. Kassambara, A. (2022). rstatix: pipe-friendly framework for basic statistical tests.. The Comprehensive R Archive Network https://cran.r-project.org/web/packages/rstatix/index.html.

96. Wickham, H. (2007). Reshaping data with the reshape package. J. Stat. Softw. *21*, 1–20. https://doi.org/10.18637/jss.v021.i12.

97. Emms, D.M., and Kelly, S. (2019). OrthoFinder: phylogenetic orthology inference for comparative genomics. Genome Biol. *20*, 238. https://doi.org/10.1186/s13059-019-1832-y.

98. Seemann, T. (2014). Prokka: rapid prokaryotic genome annotation. Bioinformatics *30*, 2068–2069. https://doi.org/10.1093/bioinformatics/btu153.

99. Jain, C., Rodriguez-R, L.M., Phillippy, A.M., Konstantinidis, K.T., and Aluru, S. (2018). High throughput ANI analysis of 90K prokaryotic genomes reveals clear species boundaries. Nat. Commun. *9*, 5114. https://doi.org/10.1038/s41467-018-07641-9.

100. Huerta-Cepas, J., Szklarczyk, D., Heller, D., Hernández-Plaza, A., Forslund, S.K., Cook, H., Mende, D.R., Letunic, I., Rattei, T., Jensen, L.J., et al. (2019). eggNOG 5.0: a hierarchical, functionally and phylogenetically annotated orthology resource based on 5090 organisms and 2502 viruses. Nucleic Acids Res. *47*, D309–D314. https://doi.org/10.1093/nar/gky1085.

101. Katz, L.S., Griswold, T., Morrison, S.S., Caravas, J.A., Zhang, S., den Bakker, H.C., Deng, X., and Carleton, H.A. (2019). Mashtree: a rapid comparison of whole genome sequence files. J. Open Source Softw. *4*, 1762. https://doi.org/10.21105/joss.01762.

102. Schindelin, J., Rueden, C.T., Hiner, M.C., and Eliceiri, K.W. (2015). The ImageJ ecosystem: an open platform for biomedical image analysis. Mol. Reprod. Dev. *82*, 518–529. https://doi.org/10.1002/mrd.22489.

103. Bray, N.L., Pimentel, H., Melsted, P., and Pachter, L. (2016). Near-optimal probabilistic RNA-seq quantification. Nat. Biotechnol. *34*, 525–527. https://doi.org/10.1038/nbt.3519.

104. Martin, M. (2011). Cutadapt removes adapter sequences from high-throughput sequencing reads. EMBnet J. *17*, 10–12. https://doi.org/10.14806/ej.17.1.200.

105. Berendsen, R.L., Vismans, G., Yu, K., Song, Y., de Jonge, R., Burgman, W.P., Burmølle, M., Herschend, J., Bakker, P.A.H.M., and Pieterse, C.M.J. (2018). Disease-induced assemblage of a plant-beneficial

bacterial consortium. ISME J. *12*, 1496–1507. https://doi.org/10.1038/s41396-018-0093-1.

106. Van Wees, S.C.M., Van Pelt, J.A., Bakker, P.A.H.M., and Pieterse, C.M.J. (2013). Bioassays for assessing jasmonate-dependent defenses triggered by pathogens, herbivorous insects, or beneficial rhizobacteria. In Jasmonate Signaling: Methods and Protocols: Volume 1011 of Methods in Molecular Biology, A. Goossens, and L. Pauwels, eds. (Humana Press), pp. 35–49. https://doi.org/10.1007/978-1-62703-414-2_4.

107. Kanehisa, M., and Goto, S. (2000). KEGG: Kyoto encyclopedia of genes and genomes. Nucleic Acids Res. *28*, 27–30. https://doi.org/10.1093/nar/28.1.27.

108. Kupferschmied, P., Péchy-Tarr, M., Imperiali, N., Maurhofer, M., and Keel, C. (2014). Domain shuffling in a sensor protein contributed to the evolution of insect pathogenicity in plant-beneficial *Pseudomonas protegens*. PLoS Pathog. *10*, e1003964, https://doi.org/10.1371/journal.ppat.1003964.

STAR★METHODS

KEY RESOURCES TABLE

REAGENT or RESOURCE	SOURCE	IDENTIFIER
Bacterial and virus strains		
CHA0 ΔiolI	This study	N/A
CHA0 ΔiolI-mCherry	This study	N/A
CHA0-gfp	This study	N/A
Critical commercial assays		
MagAttract PowerSoil DNA KF Kit	Qiagen	Cat. No. 27000-4-KF
BR dsDNA assay kit	Thermo Fisher Scientific	Cat. No. Q33211
MS medium	Duchefa Biochemie	Cat. No. M0222.0050
Deposited data		
High-throughput sequencing data (NCBI Sequence Read Archive)	This study	BioProject ID: PRJNA960651
R code and sample data (Zenodo)	This study	https://doi.org/10.5281/zenodo.7855318
Experimental models: Organisms/strains		
Bacterium: Pseudomonas simiae WCS417	Willie Commelin Scholten collection; see Table S1	N/A
Bacterium: Pseudomonas protegens CHA0	See Table S1	N/A
Bacterium: Pseudomonas capeferrum WCS358	Willie Commelin Scholten collection; see Table S1	N/A
Bacterium: Pseudomonas sp. WCS134	Willie Commelin Scholten collection; see Table S1	N/A
Bacterium: *Pseudomonas fluorescens* RS158	See Table S1	N/A
Bacterium: *Pseudomonas* sp. WCS317	Willie Commelin Scholten collection; see Table S1	N/A
Bacterium: *Salinibacter ruber*	Deutsche Sammlung von Mikroorganismen und Zellkulturen GmbH (DSMZ)	DSM 13855
Plant: *Arabidopsis thaliana* accession Col-0	N/A	N/A
Oligonucleotides		
TCGTCGGCAGCGTCAGATGTGTATAAGAGACAGTCGCCTTACCTGTGGCCTACGGGNGGCWGCAG	This study	50-NGS1-16s-N701
TCGTCGGCAGCGTCAGATGTGTATAAGAGACAGCTAGTACGGAGTGGCCTACGGGNGGCWGCAG	This study	51-NGS1-16s-N702
TCGTCGGCAGCGTCAGATGTGTATAAGAGACAGTTCTGCCTTGCGACCTACGGGNGGCWGCAG	This study	52-NGS1-16s-N703
TCGTCGGCAGCGTCAGATGTGTATAAGAGACAGGCTCAGGAATGACCTACGGGNGGCWGCAG	This study	53-NGS1-16s-N704
TCGTCGGCAGCGTCAGATGTGTATAAGAGACAGAGGAGTCCCGACCTACGGGNGGCWGCAG	This study	54-NGS1-16s-N705
TCGTCGGCAGCGTCAGATGTGTATAAGAGACAGCATGCCTACGACCTACGGGNGGCWGCAG	This study	55-NGS1-16s-N706

(*Continued on next page*)

Continued

REAGENT or RESOURCE	SOURCE	IDENTIFIER
TCGTCGGCAGCGTCAGATGTGKTATAAG AGACAGGTAGAGAGGTCCTACGGGNG GCWGCAG	This study	56-NGS1-16s-N707
TCGTCGGCAGCGTCAGATGTGTATAAGA GACAGCCTCTCTGGTCCTACGGGNGG CWGCAG	This study	57-NGS1-16s-N708
TCGTCGGCAGCGTCAGATGTGTATAAGA GACAGAGCGTAGCTCCTACGGGNGG CWGCAG	This study	58-NGS1-16s-N709
TCGTCGGCAGCGTCAGATGTGTATAAGA GACAGCAGCCTCGTCCTACGGGNGG CWGCAG	This study	59-NGS1-16s-N710
TCGTCGGCAGCGTCAGATGTGTATAAGA GACAGTGCCTCTTCCTACGGGNGGC WGCAG	This study	60-NGS1-16s-N711
TCGTCGGCAGCGTCAGATGTGTATAAGA GACAGTCCTCTACCCTACGGGNGGC WGCAG	This study	61-NGS1-16s-N712
GTCTCGTGGGCTCGGAGATGTGTATAAG AGACAGTAGATCGCCACTTCTGACTAC HVGGGTATCTAATCC	This study	62-NGS1-16s-N501
GTCTCGTGGGCTCGGAGATGTGTATAAG AGACAGCTCTCTATTTCTCTGACTACH VGGGTATCTAATCC	This study	63-NGS1-16s-N502
GTCTCGTGGGCTCGGAGATGTGTATAAG AGACAGTATCCTCTACTCAGACTACH VGGGTATCTAATCC	This study	64-NGS1-16s-N503
GTCTCGTGGGCTCGGAGATGTGTATAAG AGACAGAGAGTAGAGATAGACTACH VGGGTATCTAATCC	This study	65-NGS1-16s-N504
GTCTCGTGGGCTCGGAGATGTGTATAAG AGACAGGTAAGGAGCTA GACTACHV GGGTATCTAATCC	This study	66-NGS1-16s-N505
GTCTCGTGGGCTCGGAGATGTGTATAAG AGACAGACTGCATATC GACTACHVG GGTATCTAATCC	This study	67-NGS1-16s-N506
GTCTCGTGGGCTCGGAGATGTGTATAAG AGACAGAAGGAGTAA GACTACHVGG GTATCTAATCC	This study	68-NGS1-16s-N507
GTCTCGTGGGCTCGGAGATGTGTATAAG AGACAGCTAAGCCT GACTACHVGGG TATCTAATCC	This study	69-NGS1-16s-N508
cgGAATTCctgctcaaggacctgaaa	This study	del-iol-1
cggGGTACCttcgacgactagcccttc	This study	del-iol-2
cggGGTACCgcctatgacgtcgagctg	This study	del-iol-3
cgGGATCCcgccactcggttctgaat	This study	del-iol-4
cttgagcgatgtgcagat	This study	check-iol-F
ttctttgtgcagaagccg	This study	check-iol-R
Recombinant DNA		
pSEVA212S; *ori*R6K, *lacZ*α with two flanking I-SceI sites; Km^R, Ap^R	Martínez-García and de Lorenzo[65]	pEMG
*ori*RK2, *xylS*, P_m::*I-sce*I; Gm^R	Martínez-García and de Lorenzo[65]	pSW-2

(*Continued on next page*)

Continued		
REAGENT or RESOURCE	SOURCE	IDENTIFIER
pME11149; suicide plasmid for the in-frame deletion of the *iol* cluster (PPRCHA0_2627 to PPRCHA0_2633)	This study	pEMG::Δ*iol*
Software and algorithms		
R	R Core Team[66]	4.2.2
ggplot2	Wickham[67]	3.4.1
ggpubr	Kassambara[68]	0.5.0
ggVennDiagram	Gao[69]	1.2.2
KEGGREST	Tenenbraum, [70]	1.38.0
dada2	Callahan et al.[71]	1.26.0
multcomp	Hothorn et al.[72]	1.4.22
dplyr	Wickham et al.[73]	1.0.10
MASS	Venables and Ripley[74]	7.3.57
emmeans	Lenth[75]	1.8.4
magrittr	Bache and Wickham[76]	2.0.3
ggtext	Wilke and Wiernik[77]	0.1.2
patchwork	Pedersen[78]	1.1.2
ggsci	Xiao[79]	2.9
ggnet	Briatte[80]	0.1.0
network	Butts et al.[81]	1.13.0.1
growthcurver	Sprouffske[82]	0.3.1
Hmisc	Harrell[83]	4.7-2
pheatmap	Kolde[84]	1.0.12
scales	Wickham and Seidel[85]	1.2.1
extrafont	Chang[86]	0.19
assertthat	Wickham[87]	0.2.1
Biostrings	Pagès et al.[88]	2.66.0
PerformanceAnalytics	Peterson and Carl[89]	2.0.4
stringr	Wickham and Rstudio[90]	1.5.0
magick	Ooms[91]	2.7.3
readxl	Wickham and Bryan[92]	1.4.1
ggrepel	Slowikowski[93]	0.9.2
tidyr	Wickham et al.[94]	1.3.0
rstatix	Kassambara[95]	0.7.1
reshape2	Wickham[96]	4.2.2
OrthoFinder	Emms and Kelly[97]	2.5.4
Prokka	Seemann[98]	1.14.6
fastANI	Jain et al.[99]	1.33
eggNOG-mapper	Huerta-Cepas et al.[100]	2.1.8
cblaster	Gilchrist et al.[18]	1.3.17
mashtree	Katz et al.[101]	1.2.0
ImageJ	Schindelin et al.[102]	1.53
kallisto	Bray et al.[103]	0.45.0
cutadapt	Martin[104]	2.8

RESOURCE AVAILABILITY

Lead contact

Requests for resources or information should be directed to Ronnie de Jonge (r.dejonge@uu.nl).

Materials availability

This study did not generate new unique reagents.

Data and code availability

- The raw *16S rRNA* amplicon sequencing data and genomes in this study have been deposited at NCBI Sequence Read Archive (BioProject: PRJNA960651) and are publicly available as of the date of publication. The accession number is listed in the key resources table.
- The R code and data, both the data generated here and the public data used to generate Figure 7, have been deposited at Zenodo (https://doi.org/10.5281/zenodo.7855318) and are publicly available as of the date of publication. The DOI is listed in the key resources table.
- Any additional information required to reanalyze the data reported in this paper is available from the lead contact upon request.

EXPERIMENTAL MODEL AND SUBJECT DETAILS

Arabidopsis thaliana

Seeds of Arabidopsis accession Col-0 were surface-sterilized with chlorine gas in a glass chamber and subsequently aerated in a flow cabinet to remove the residual chlorine for 30 min. Sterile seeds were sown in agar plates containing 1x Murashige and Skoog (MS) medium (Duchefa Biochemie) supplemented with 0.5% sucrose. Plates were sealed twice with parafilm, let stratify for 48 h at 4°C, and positioned vertically in a growth chamber under short-day conditions for two weeks (22 °C; 10 h light/14 h dark; light intensity 100 μmol/m^2/s).

Bacterial cultures

All pseudomonads are cultured on King's B (KB) medium plates (2% proteose peptone, 8.6 mM K_2HPO_4, 6.1 mM $MgSO_4 \cdot 7H_20$, 1% v/v glycerol) agar plates and incubated overnight at 28 °C. A live aliquot of *Salinibacter ruber* M31 was grown for 14 days in liquid Medium 936 for *S. ruber* as prescribed by DSMZ (3.3 M NaCl, 200 mM $MgSO_4$ x 7 H_2O, 170 mM $MgCl_2$ x 6 H_2O, 8.5 mM $CaCl_2$ x 2 H_2O, 67 mM KCl, 3 mM $NaHCO_3$, 6 mM NaBr, 1 g/l yeast extract, pH 7.2) at 37 °C and 100 rpm.

METHOD DETAILS

Soil treatments, transplantations, and microbiome sampling

A schematic representation of the experimental design can be seen in Figure S1. Per isolate, single colonies were spread onto five KB plates and incubated overnight at 28 °C. Per plate, 5 ml of $MgSO_4$ 10 mM was used to scrape the microbial cell layer off the surface, and the resulting suspension was collected into 50-ml tubes for every isolate. The cell suspension was washed thrice by centrifugation at 3000 x g for 10 min, resuspending in 40-50 ml $MgSO_4$ 10 mM every step. The final cell pellet was resuspended in 20 ml of $MgSO_4$ 10 mM, and the bacterial density was measured by determining the optical density (OD) at 600 nm (equivalence: 1 OD_{600} unit, $8 \cdot 10^8$ CFU/ml).

In this study we used top soil collected from the Reijerscamp natural reserve (52°01′02.55″, 5°77′99.83″, Wolfheze, Netherlands), a gleyic placic podzol consisting of coarse sand and gravel where natural Arabidopsis populations occur and that has been previously used for microbiome studies in Arabidopsis.[105] The soil was dried, sieved to remove large gravel, and inoculated with each microbial suspension to reach an inoculum density of 10^8 CFU/g of soil in a final volume of 100 ml/kg of soil. For the mock treatment, the soil was moistened with $MgSO_4$ 10 mM at 100 ml/kg of soil. This initial inoculum density was decided based on the detection limit of our spike-in method in preliminary assessments of the technique. Given a total *Salinibacter* spike-in abundance of $9.84 \cdot 10^5$ copies per sample, we calculated the density detection limit by dividing this abundance by sample weight. In our experiment, this resulted in an average detection limit across samples of $2.1 \cdot 10^4 \pm 2.5 \cdot 10^3$ CFU/g, with certain samples showing a detection limit up to 10^6 CFU/g (Figure S7), indicating that the initial inoculation density had to be higher than 10^6 CFU/g in order to ensure reliable quantifications of our inoculants. Therefore, and also to account for the possibility that the density of some microbes could significantly decrease in time, we decided to use an initial inoculum density of 10^8 CFU/g as previously reported in other assays.[106]

Per inoculation treatment, 12 two-weeks-old Arabidopsis seedlings were transferred to individual pots (diameter = 5.5 cm and height = 5 cm; MXC5,5 Pöppelmann) containing 100 g of inoculated Reijerscamp soil each. All pots were placed on trays on individual Petri dishes to prevent cross-contaminations and kept in the growth chamber under the same conditions as mentioned above. The trays were kept closed with a lid for the first two days post-transplantation. For the remaining time of the cultivation period, the lids were removed, and the plants were watered every two days with 5-10 ml of tap water. Roots were eventually harvested at 21 dpi (5 weeks-old) and processed in two different ways to obtain the different plant fractions. For rhizosphere samples, roots were washed in 50-ml tubes with 30 ml sterile 10 mM $MgSO_4$ by inverting the tube 10 times. For root samples, roots were instead washed twice in 50-ml tubes by vortexing 15 s in 30 ml sterile phosphate-Silwet buffer (PBS-S; 137 mM NaCl, 10 mM Na_2HPO_4, 1.8 mM KH_2PO_4, 2.7 KCl, 0.02% Silwet). Roots cleaned with both methods, representing different fraction samples, were retrieved with sterile tweezers, tapped dry on clean paper, and transferred to 2-ml tubes containing 1 ml $MgSO_4$ 10 mM with two glass beads. For soil samples, we

collected approximately 0.25 g of soil from unplanted pots. Every fraction (soil, rhizosphere, and root) consisted of four replicates. Sample weight was obtained by weighing the tubes before and after collecting the sample. The tubes were shaken twice at 20 Hz in a TissueLyser, snap frozen in liquid nitrogen, and stored at -80°C until DNA extractions. This experiment to screen for superior root colonization was performed once.

DNA extractions, *16S rRNA* amplicon library preparation, and data normalization

Nucleic acid extractions from all sample types were performed on a KingFisher Flex (Thermo Fisher Scientific) using a protocol based on the MagAttract PowerSoil DNA KF Kit. The resulting DNA was quantified with Qubit fluorometric quantitation (Invitrogen) with the BR dsDNA assay kit (Thermo Fisher Scientific).

In order to obtain absolute counts of each isolate, we used DNA from *Salinibacter ruber* (*Salinibacter*), an extreme halophile found in saltern crystallizer ponds that is not found in our samples and that encodes a single *16S rRNA* gene copy in its genome. Based on the genome size of 3.6 Mbp (GenBank accession ID GCA_000013045.1), we calculated an expected copy number of 2.46•105 chromosomes per nanogram of genomic DNA, with an equivalent number of copies of the *16S rRNA* gene. Cell lysis buffer was spiked with 4 ng of *S. ruber* DNA per sample, aiming at a final concentration of 0.1-1% of the total amount of DNA. Library preparation was conducted according to Illumina's 16S Sequencing Library Preparation protocol, using phasing primers for the V3-V4 region (Table S2). The final libraries were quantified using Qubit fluorometric quantitation with the BR dsDNA assay kit, pooled at a sample concentration of 4 nM, and sequenced on Illumina MiSeq to obtain 2x300 bp paired-end reads.

The resulting reads were processed using cutadapt[104] and the DADA2 pipeline.[71] To increase sensitivity of the DADA2 pipeline for the introduced isolates and their respective *16S rRNA* sequences, we used the known V3-V4 region of the isolates, plant mitochondrion, plant chloroplast, and *Salinibacter* as priors in the amplicon sequence variant (ASV) inference step. For every inoculation treatment, ASVs were inferred from all treated samples and mock samples by prioring with the sequence of the respective isolate, plant, and *Salinibacter*. Sequences used as priors are listed in Table S2.

After removal of chimeric sequences, the counts of every isolate were normalized with respect to the counts of *Salinibacter* by taking the ratio of isolate counts to the observed *Salinibacter* counts, and multiplying this ratio by the total number of added *Salinibacter* copies in the sample preparation (4 ng/sample • $2.46 \cdot 10^5$ 16S gene copies/ng, $9.84 \cdot 10^5$ copies/sample). Final microbial densities are calculated by normalizing estimated *16S rRNA* copy numbers with plant weight and subtracting counts from uninoculated samples when applicable, i.e., for WCS417 and WCS358. Figure S3 shows the raw densities used to generate Figure 1 before subtraction of the density in uninoculated samples.

Genomic analysis

To identify genes that could potentially explain the enhanced colonization ability in *P. simiae* WCS417 and *P. protegens* CHA0, we subjected the genomes of all isolates to a comparative genetic analysis based on presence/absence of orthologs (Figure S2). First, proteomes were inferred from the genome sequences using Prokka.[98] The proteomes were then used as input for OrthoFinder[97] in order to infer phylogenetic relationships among all genes and group them into orthologous protein families or orthogroups. The result is a table of all orthogroups inferred and a list of its orthologues found in each individual genome. In parallel, all proteomes were annotated using the eggNOG-mapper[100] and the KEGG database.[107] Enriched functions in the set of orthologues shared by only WCS417 and CHA0 were identified by a Fisher's exact test by comparing the functions of these orthologues with those in the complete proteomes.

Mutant construction

Deletion of the entire *iol* gene cluster (from PPRCHA0_2627 to PPRCHA0_2633, i.e., from *iolR* to *iolG*) was generated by homologous recombination using the suicide vector pEMG and the I-SceI system adapted to *P. protegens*.[108] Briefly, the pEMG::Δ*iol* vector for homologous recombination was constructed by fusing a fragment upstream with a fragment downstream of the *iol* locus, amplified with primers del-iol-1/del-iol-2 and del-iol-3/del-iol-4, respectively, and cloning the resulting fused fragment into pEMG. Competent CHA0 cells were electroporated with pEMG::Δ*iol* and successful insertional mutants were selected on Luria-Bertani (LB) plates supplemented with 25 μg/ml kanamycin. Competent mutant cells were subsequently transformed with the expression plasmid pSW-2 by electroporation and selected for gentamicin resistance on LB plates supplemented with 10 μg/ml gentamicin. Individual colonies were grown overnight at 30°C in liquid LB supplemented with 10 μg/ml gentamicin. Two milliliters of the overnight culture were transferred to 10 ml of fresh LB supplemented with 2 mM m-toluate and 10 μg/ml gentamicin and incubated for 7 h at 30°C to allow a second homologous recombination event. Dilutions of bacterial cultures were plated on LB plates without antibiotics and isolated colonies were screened for kanamycin sensitivity. Mutants were identified by specific PCR and sequencing of the respective genomic region with primers check-iol-F and check-iol-R.

Root colonization and competition assays

Experiments with *gfp*-tagged CHA0 WT and *mCherry*-tagged mutant were performed as described previously for the isolates comparisons, with minor differences. Individual inoculations were performed at the same microbial density as described, 10^8 CFU/g soil, while mixed inoculations contained $0.5 \cdot 10^8$ CFU/g of each isolate, in order to obtain a comparable total microbial density as in individual inoculations. At 21 dpi, only root and not rhizosphere samples were collected. Instead of freezing, 10-fold dilutions of the

shaken supernatant were plated on KB agar plates supplemented with 10 μg/ml gentamicin and incubated overnight at 28°C. Root microbial density was calculated by normalizing CFU counts by root fresh weight.

Growth assays

For planktonic growth, overnight cultures of CHA0 WT and the Δiol mutant were diluted 1/10 in fresh, liquid KB medium and grown 4 h in order to synchronize both genotypes in the exponential phase. The cell suspension was washed thrice by centrifugation at 3,000 x g, decanting of the supernatant, and resuspension in the respective medium. Cells were inoculated individually in flat-bottom 96-well plates at a final OD_{600} equal to 0.01 in either M9 for the assessment of sole carbon sources (26 mM Na_2HPO_4,•$7H_20$, 11 mM KH_2PO_4, 4.3 mM NaCl, 9.3 mM NH_4Cl) or 0.1X Cook's Cytophaga (CC) to study the effect of inositol addition on growth (0.2% tryptone). For assessment of inositol as a carbon source, the medium was left unsupplemented or supplemented with 100 mM of glucose or inositol. For assaying effects of inositol on growth, medium was left unsupplemented or supplemented with 10 mM glucose or inositol.

Growth curves were obtained by measuring OD_{600} every 30 min in a plate reader (Synergy H1, BioTek) for 72 h (inositol usage as carbon source) or 48 h (inositol effects on growth). Growth curve analyses were done with the *growthcurver* package in R.[82]

Motility assays and siderophore plates

Swimming and swarming motility were assayed in 0.1X Cook's Cytophaga-agar (CCA) minimal medium at 0.3% or 0.5%, respectively. For all assays, the medium was supplemented with inositol or glucose as a control carbon source at 1 or 10 mM or left unsupplemented. Cells were prepared as for growth experiments. For the swimming assay, sterile pipette tips were dipped in the cell suspension and the agar was gently pierced until reaching the middle of the agar, and without reaching the bottom. Pictures were taken after 48 h of growth at 21°C and analyzed with ImageJ.[102] The swimming halo radii and diameters were used to assess swimming motility. For swarming, 1 μl of bacterial suspension was carefully inoculated on the agar surface and avoiding damage of the agar. Pictures were taken at the same time points as for swimming, and swarming ability was measured as the surface area covered by bacteria. In both assays, we inoculated CHA0 WT, CHA0 Δ*iol*, and two previously reported spontaneous CHA0 mutant that exhibit promoted swimming motility as positive control (*sadB*), and impaired swimming as negative control (*fleQ*).[17] Every treatment consisted of 20 replicate plates and all experiments were repeated at least twice.

Siderophore plates followed the same procedure as swimming plates, using 1X CC medium. In order to ensure that all inoculations were performed at the same distance from each other, they were all done by dipping five pipette tips in a cell suspension with a multichannel pipette and inserting the pipette tips until the center of the agar, as described for swimming inoculations. Every treatment consisted of three replicates and was repeated twice.

Analyses on publicly available data

For the analysis of *in vitro* genome-wide fitness data of root colonization in WCS417, we used supplementary data from Cole et al.[19] and selected the genes in the *iol* locus in WCS417 (*iolR*, PS417_11845; *iolC*, PS417_11850; *iolD*, PS417_11855; *iolE*, PS417_11860; *iolB*, PS417_11865; *iolI*, PS417_11870; *iolD*, PS417_11875; *iolG*, PS417_11880; *mocA*, PS417_11885; *iatA*, PS417_11890; *iatC*, PS417_11895; *iatB* PS417_11900). For the analysis of genome-wide fitness data of WCS417 in different conditions, we retrieved the data from Price et al.[20] available in Fitness Browser (https://fit.genomics.lbl.gov/cgi-bin/help.cgi). We kept all experimental conditions in which any of the genes in the *iol* locus of WCS417 was affected with a *t*-like score and a fitness value greater than 0.5. For the remaining conditions with more than one repeat, we took the median fitness value. We built a bipartite network of genes and conditions according to the fitness values using the *network*[81] and *ggnet*,[80] R packages for construction and visualization, respectively. For the network representation, we used the Fruchterman-Reingold algorithm with 1,000 iterations and an area and repulsion radius of 30,000,000. For the analysis of transcriptional activity of CHA0 in the host, we retrieved sequenced data from Vesga et al.[21] from the NCBI database (BioProject accession PRJNA595077) and mapped the reads to the CHA0 genome (assembly GCF_900560965.1) with kallisto v0.45.0.[103] Transcripts-per-million values for each gene were log_2-transformed and scaled per gene.

QUANTIFICATION AND STATISTICAL ANALYSIS

The R programming environment (version 4.2.2) was used for data analysis and visualization. All statistical tests were performed in R. All details about the statistical analyses, sample numbers and biological replicates are provided in the figure legends and respective methods section.

Current Biology, Volume *33*

Supplemental Information

The conserved *iol* gene cluster in *Pseudomonas* is involved in rhizosphere competence

Juan J. Sánchez-Gil, Sanne W.M. Poppeliers, Jordan Vacheron, Hao Zhang, Bart Odijk, Christoph Keel, and Ronnie de Jonge

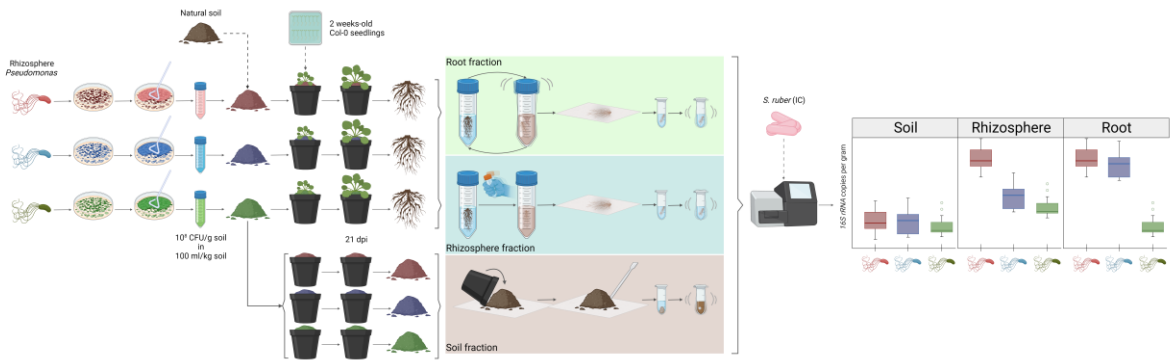

Figure S1. Schematic representation of the experimental design. Related to Figure 1 and STAR Methods. Root-associated pseudomonads are mixed through natural soil and let to colonise Arabidopsis roots for 21 days. Rhizosphere and root samples are collected and mixed with DNA of *Salinibacter ruber* as internal control. Absolute population density of each pseudomonad is calculated by sequencing the *16S rRNA* gene and normalising the counts with the internal control and the sample weight. Created with BioRender.com.

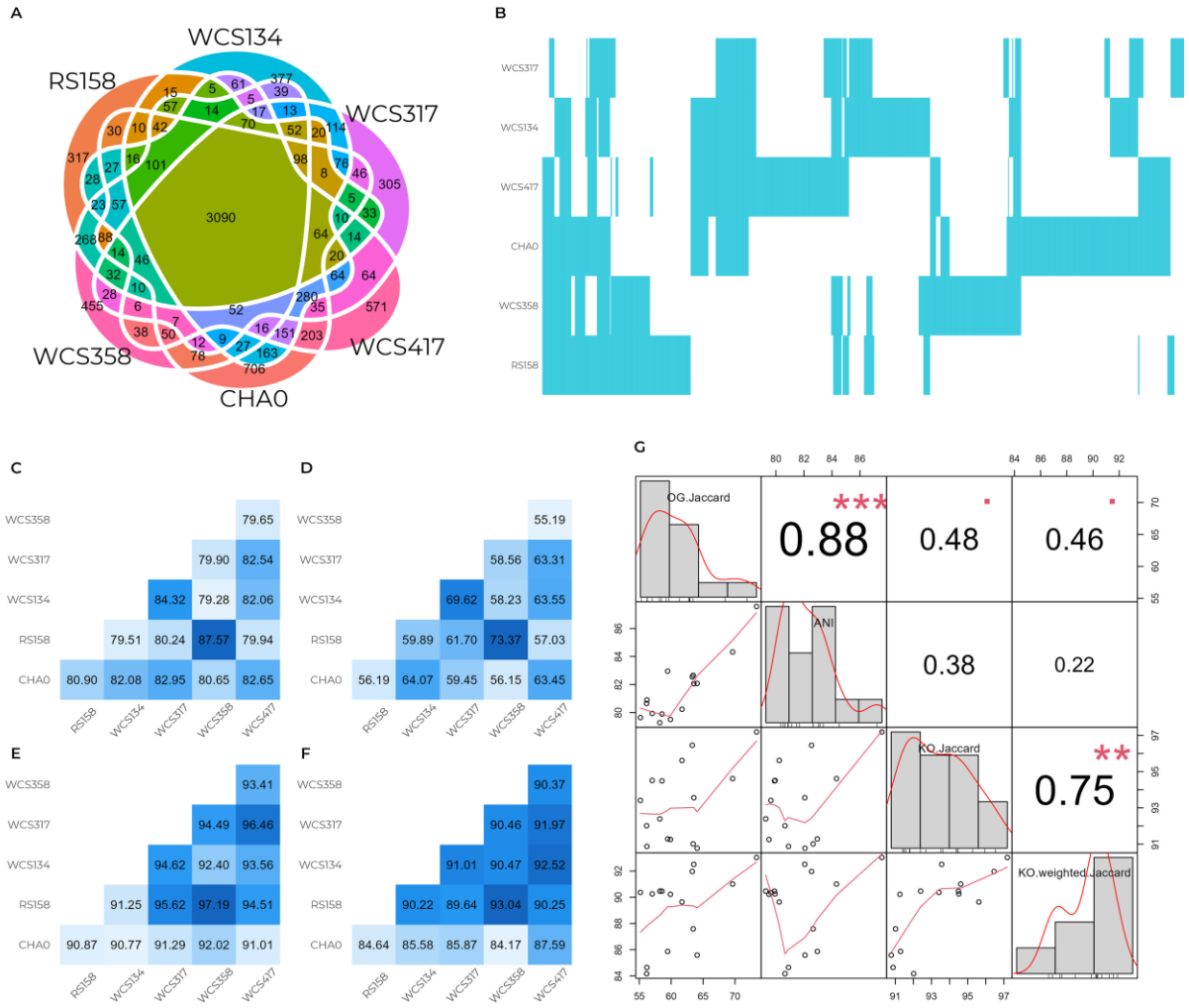

Figure S2. The isolates in this study are a diverse set of root-associated pseudomonads. Related to Figure 1 and STAR Methods. (A) Venn diagram showing the relationship of ortholog group presence-absence among isolates' genomes. Out of 8,752 orthogroups, 3,090 (35%) are shared by all isolates. (B) Distribution of the non-core genes. (C) Pair-wise average nucleotide identity (ANI) among isolates. (D) Pair-wise unweighted Jaccard similarity of the orthogroup presence-absence per genome (i.e., percentage of shared genes between isolate pairs). (E) Pair-wise unweighted Jaccard similarity of KEGG pathway annotations per genome. The relatively high values suggest that the functional capabilities of the isolates are very similar. (F) Same as E, but showing the weighted Jaccard similarity between the compositions of pathway annotations. The differences in the weighted vs unweighted metric indicate that certain functions encoded in the genomes do not distribute evenly between them, highlighting the functional diversity in the genomes. (G) Pair-wise correlation plots of the previously shown metrics in C-F.

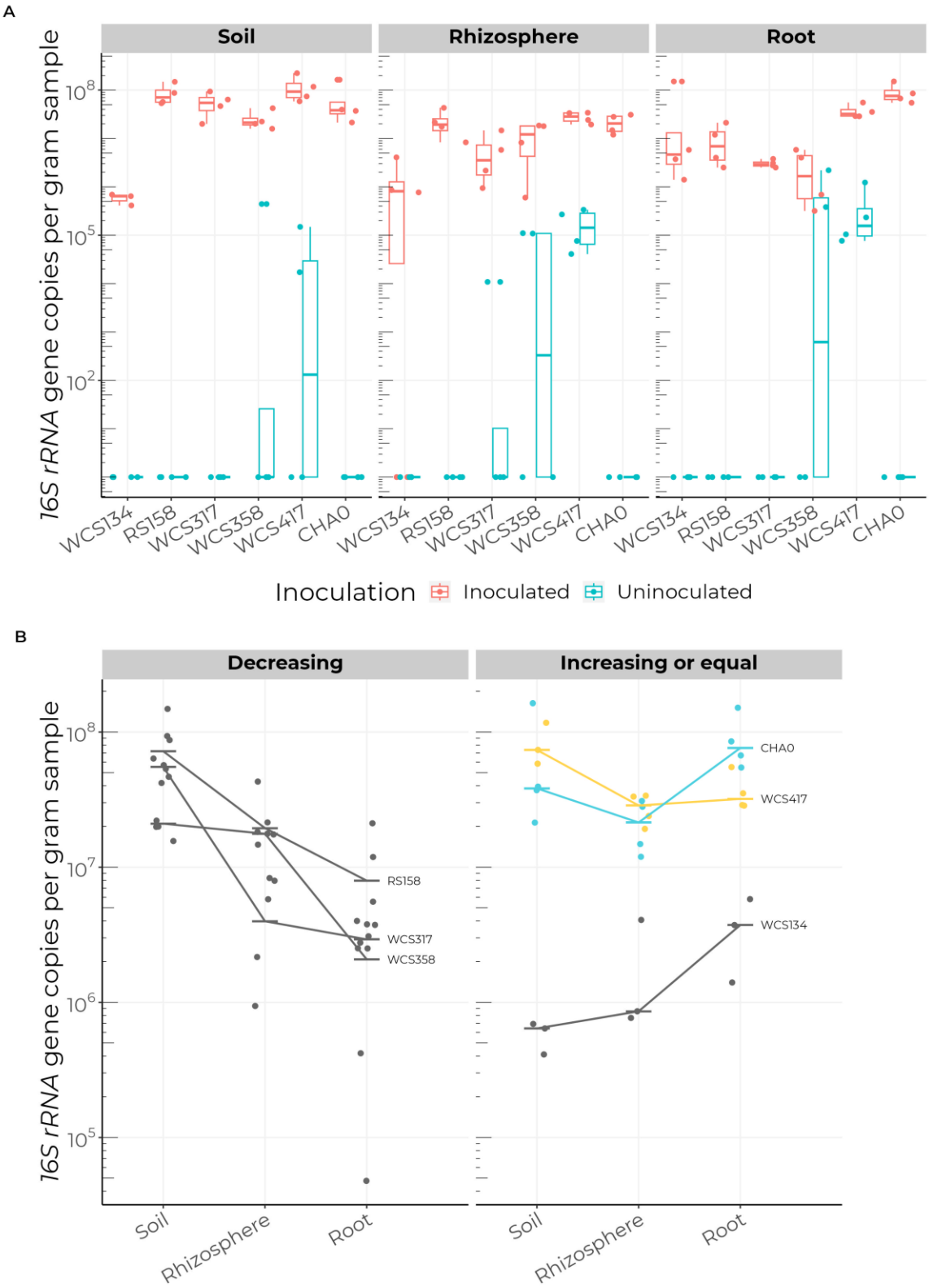

Figure S3. Raw microbial densities and isolate densities across fractions. Related to Figure 1. (A) Absolute inoculum densities at 21 dpi, for both inoculated and uninoculated samples, previous to the subtraction of counts in uninoculated samples as in Figure 1. (B) Absolute inoculum densities after 21 dpi measured as the number of *16S rRNA* copies per gram of sample found in bulk soil (left), rhizosphere (middle), and root samples (right). *P. protegens* CHA0 and *P. simiae* WCS417 are highlighted in cyan and yellow, respectively,

to differentiate them from the remaining isolates. The density of some isolates decreases in the root (RS158, WCS317, and WCS358), while others increase or remain equal (WCS417, CHA0, and WCS134).

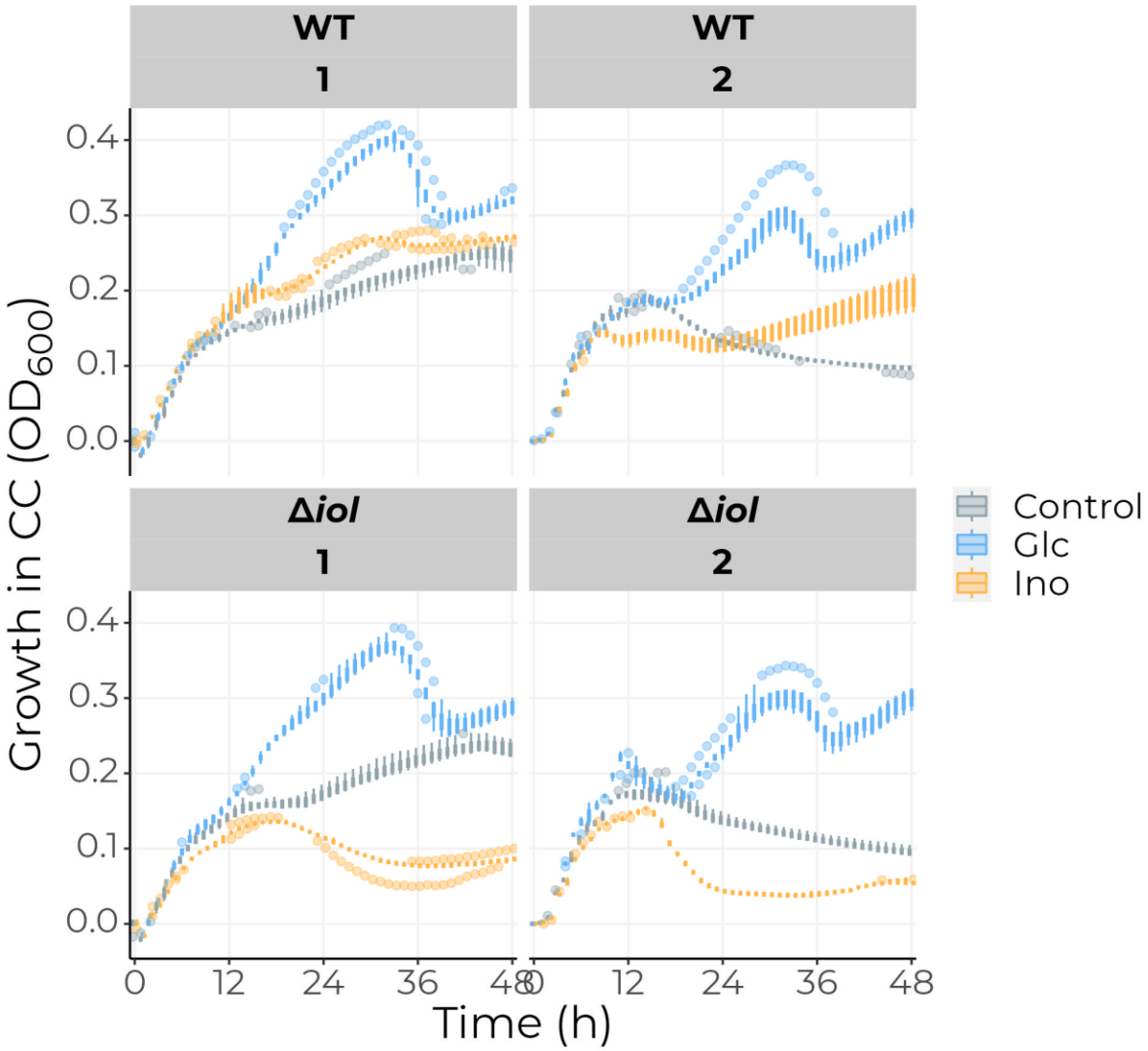

Figure S4. Inositol effects on WT cells are highly variable. Related to Figure 4. Growth curves of WT and Δ*iol* cells in CC medium unsupplemented or supplemented with 10 mM glucose or inositol, measured as OD at 600 nm. The figure shows two examples of independent experiments. The effects of inositol in the WT are clearly variable per experiment, and the benefit of inositol on growth is only apparent in some cases. Every time point consists of measurements for seven technical replicates.

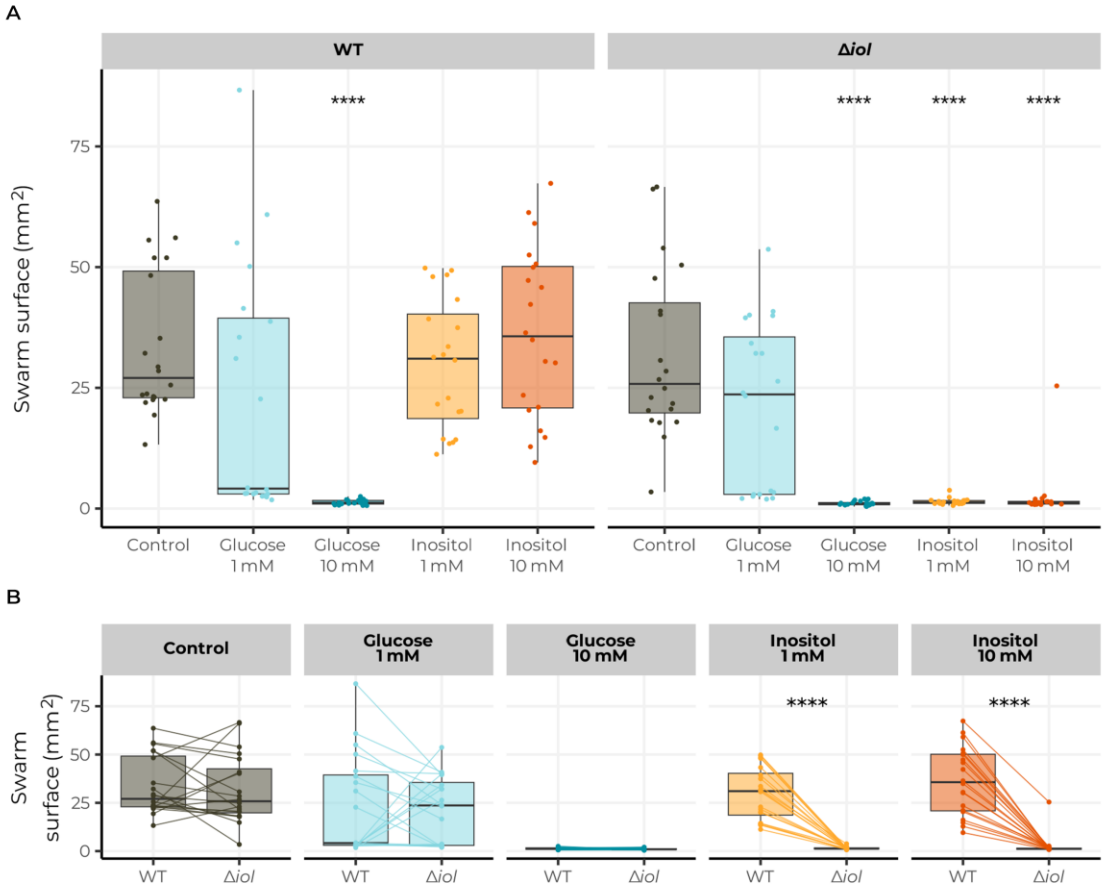

Figure S5. Inositol represses swarming motility in mutant cells. Related to Figure 5. (A) Swarming surface of WT (left) and Δ*iol* cells (right) in CC medium either unsupplemented or supplemented with glucose or inositol at 1 or 10 mM. Inositol does not seem to affect swarming motility in WT cells, while swarming is abolished in the mutant. (B) Same data as in A shown per treatment and pairing the swarming surface for both genotypes per plate, showing the difference in motility.

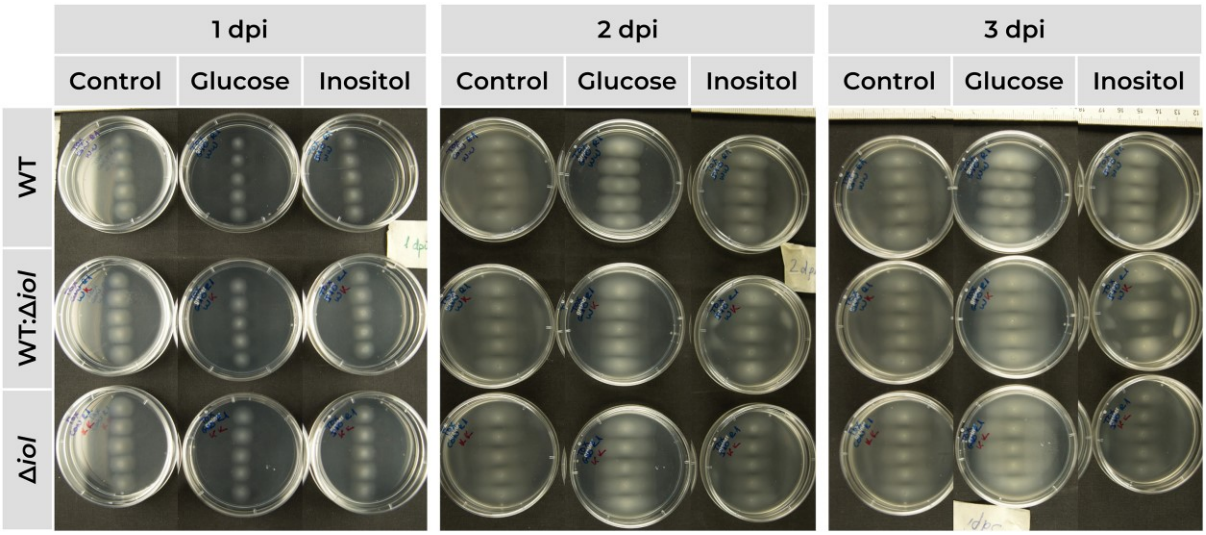

Figure S6. Inositol affects mutant physiology. Related to Figure 6. Qualitative assessment of the effect of inositol and glucose on WT and mutant cells. Images show the same plates as in Figure 6 at 1, 2, and 3 dpi. Per day, the figure shows the plates organized as follows. First column: control conditions; second column: glucose 10 mM; third column: inositol 10 mM; first row: WT cells only; second row: combination of WT and mutant cells (WT, Δ*iol*, WT, Δ*iol*, WT); third row: mutant cells only. Mutant colonies start fading after reaching the end of the plate at approximately the end of the second day.

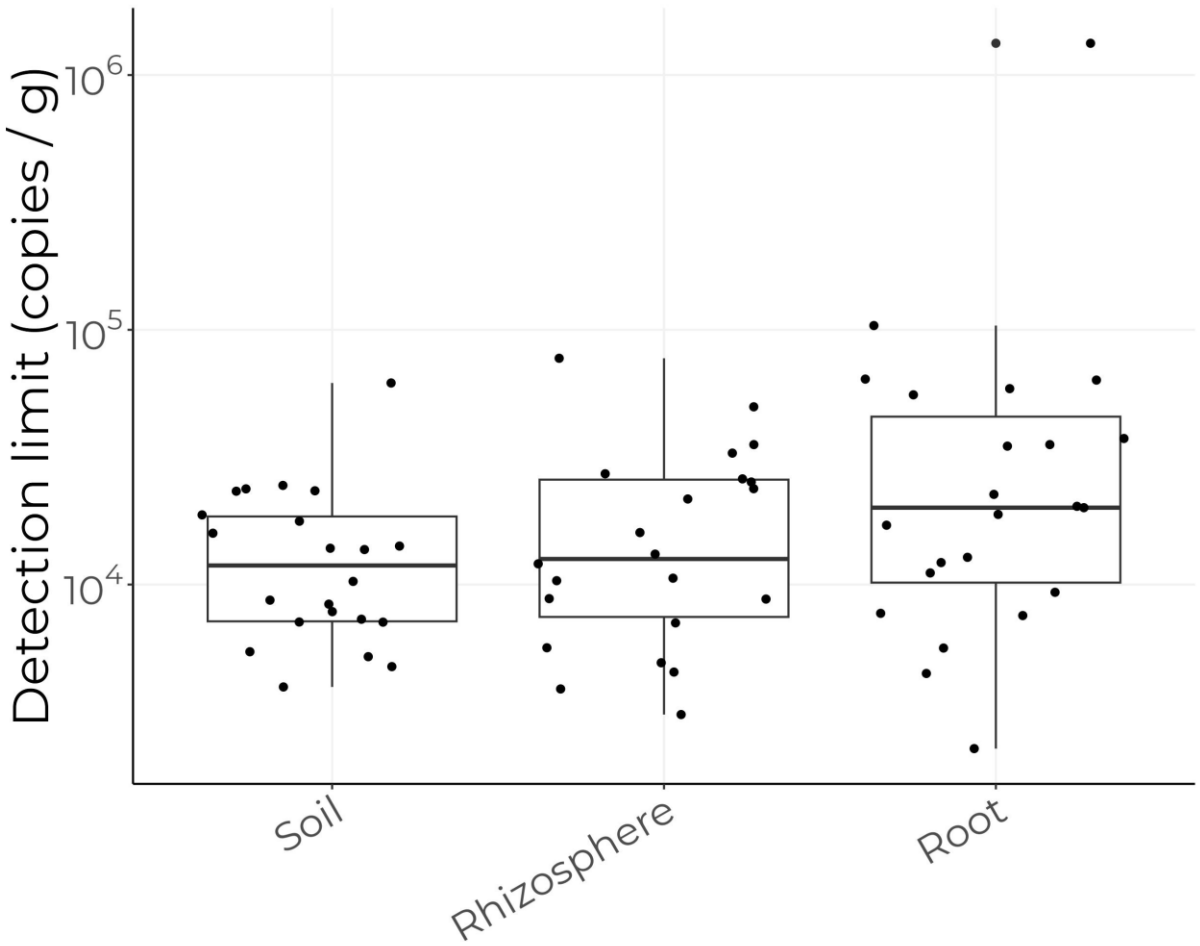

Figure S7. Detection limit of microbial density. Related to STAR Methods. Boxplot depicting the detection limit of microbial density in our spike-in method, using the minimum detectable *16S rRNA* gene copies per gram of sample.

Name	Origin	When	Where*	Effect on host**	References
***P. simiae* WCS417**	Wheat rhizosphere	1983	NL	GP, ISR	Pieterse et al., 2021[S1]
***P. protegens* CHA0**	Tobacco rhizosphere	1986	SZ	ISR, BA	Stutz et al., 1986[S2]
***P. capeferrum* WCS358**	Potato rhizosphere	1981	NL	ISR, BA	Berendsen et al., 2015; de Boer et al., 1999[S3,S4]
***P.* sp. WCS134**	Wheat rhizosphere	1983	NL	BA	de Weger et al, 1986[S5]
***P. fluorescens* RS158**	Radish rhizosphere	1987	NL	BA	de Boer et al., 1999[S4]
***P.* sp. WCS317**	Potato rhizosphere	1981	NL	ND	de Weger et al., 1986; Geels and Schippers, 1983[S5,,S6]

Table S1. Isolates used in this study. Related to Figure 1. *NL, Netherlands; SZ, Switzerland. **GP, growth promotion; ISR, induced systemic resistance; BA, biocontrol agent; ND, not determined.

Name	Sequence
Salinibacter-V3V4	TGGGGAATCTTGCACAATGGGGTCACCCCTGATGCAGCCATGCCGCGTGGAGGAAGACACC CCTATGGGGCGTAAACTCCTTTTCTGAATGAAGAAACCCCTGTAGCTTCAGGGCGCGACGGT AGTTCAGGAATAAGCACCGGCTAACTCCGTGCCAGCAGCCGCGGTAATACGGAGGGTGCAA GCGTTGTCCGGAATCACTGGGTGTAAAGGGTGTGCAGGCGGGGCAGCAAGTCGGATGTGAA ACCCCATGGCTTAACCATGGAGGTGCATTCGAAACTGTTGCTCTTGAGTCCCGGAGAGGCTGT CGGAATTCGTGGTGTAGCGGTGAAATGCGTAGATATCACGAGGAACACCAGAGGCGAAAGC GGACAGCTGGACGGGTACTGACGCTCAGGCACGAAAGCGTGGGGAGCAAACA
Mitochondrion-V3V4	TGGGGAATCTTGGACAATGGGCGAAAGCCCGATCCAGCAATATCGCGTGAGTGAAGAAAGG CAATGCCGCTTGTAAAGCTCTTTCGTCGAGTGCGCGATCATGACAGGACTCGAGGAAGAAGC CCCGGCTAACTCCGTGCCAGCAGCCGCGGTAAAACGGGGGGGGCAAGTGTTCTTCGGAATG ACTGGGCGTAAAGGGCACGTAGGCGGTGAATCGGGTTGAAAGTGAAAGTCGCCAAAAAGTG GCGGAATGCTTTCGAAACCAATTCACTTGAGTGAGACAGAGGAGAGTGGAATTTCGTGTGGA GGGGTGAAATCTACAGATCTACGAAGGAACGCCAAAAGCGAAGGCAGCTCTCTGGGTCCCT ACCGACGCTGGGGTGCGAAAGCATGGGGAGCGAACG
Chloroplast-V3V4	TGGGGAATTTTCCGCAATGGGCGAAAGCCTGACGGAGCAATGCCGCGTGGAGGTAGAAGGC CTACGGGTCCTGAACTTCTTTTCCCAGAGAAGAAGCAATGACGGTATCTGGGGAATAAGCATC GGCTAACTCTGTGCCAGCAGCCGCGGTAATACAGAGGATGCAAGCGTTATCCGGAATGATTG GGCGTAAAGCGTCTGTAGGTGGCTTTTTAAGTCCGCCGTCAAATCCCAGGGCTCAACCCTGG ACAGGCGGTGGAAACTACCAAGCTTGAGTACGGTAGGGGCAGAGGGAATTTCCGGTGGAGC GGTGAAATGCGTAGAGATCGGAAAGAACACCAACGGCGAAAGCACTCTGCTGGGCCGACAC TGACACTGAGAGACGAAAGCTAGGGGAGCGAATG
RS158-V3V4	TGGGGAATATTGGACAATGGGCGAAAGCCTGATCCAGCCATGCCGCGTGTGTGAAGAAGGT CTTCGGATTGTAAAGCACTTTAAGTTGGGAGGAAGGGCAGTAAGTTAATACCTTGCTGTTTTGA CGTTACCGACAGAATAAGCACCGGCTAACTCTGTGCCAGCAGCCGCGGTAATACAGAGGGT GCAAGCGTTAATCGGAATTACTGGGCGTAAAGCGCGCGTAGGTGGTTCGTTAAGTTGGATGT GAAAGCCCCGGGCTCAACCTGGGAACTGCATCCAAAACTGGCGAGCTAGAGTACGGTAGAG GGTGGTGGAATTTCCTGTGTAGCGGTGAAATGCGTAGATATAGGAAGGAACACCAGTGGCGA AGGCGACCACCTGGACTGATACTGACACTGAGGTGCGAAAGCGTGGGGAGCAAACA
WCS134-V3V4	TGGGGAATATTGGACAATGGGCGAAAGCCTGATCCAGCCATGCCGCGTGTGTGAAGAAGGT CTTCGGATTGTAAAGCACTTTAAGTTGGGAGGAAGGGTTGTAGATTAATACTCTGCAATTTTGA CGTTACCGACAGAATAAGCACCGGCTAACTCTGTGCCAGCAGCCGCGGTAATACAGAGGGT GCAAGCGTTAATCGGAATTACTGGGCGTAAAGCGCGCGTAGGTGGTTCGTTAAGTTGGATGT GAAATCCCCGGGCTCAACCTGGGAACTGCATTCAAAACTGTCGAGCTAGAGTATGGTAGAGG GTGGTGGAATTTCCTGTGTAGCGGTGAAATGCGTAGATATAGGAAGGAACACCAGTGGCGAA GGCGACCACCTGGACTGATACTGACACTGAGGTGCGAAAGCGTGGGGAGCAAACA
WCS317-V3V4	TGGGGAATATTGGACAATGGGCGAAAGCCTGATCCAGCCATGCCGCGTGTGTGAAGAAGGT CTTCGGATTGTAAAGCACTTTAAGTTGGGAGGAAGGGTTGTAGATTAATACTCTGCAATTTTGA CGTTACCGACAGAATAAGCACCGGCTAACTCTGTGCCAGCAGCCGCGGTAATACAGAGGGT GCAAGCGTTAATCGGAATTACTGGGCGTAAAGCGCGCGTAGGTGGTTTGTTAAGTTGGATGTG AAAGCCCCGGGCTCAACCTGGGAACTGCATTCAAAACTGACAAGCTAGAGTATGGTAGAGG GTGGTGGAATTTCCTGTGTAGCGGTGAAATGCGTAGATATAGGAAGGAACACCAGTGGCGAA GGCGACCACCTGGACTGATACTGACACTGAGGTGCGAAAGCGTGGGGAGCAAACA
WCS358-V3V4	TGGGGAATATTGGACAATGGGCGAAAGCCTGATCCAGCCATGCCGCGTGTGTGAAGAAGGT CTTCGGATTGTAAAGCACTTTAAGTTGGGAGGAAGGGCAGTAAGCGAATACCTTGCTGTTTTG ACGTTACCGACAGAATAAGCACCGGCTAACTCTGTGCCAGCAGCCGCGGTAATACAGAGGG TGCAAGCGTTAATCGGAATTACTGGGCGTAAAGCGCGCGTAGGTGGTTTGTTAAGTTGAATGT GAAAGCCCCGGGCTCAACCTGGGAACTGCATCCAAAACTGGCAAGCTAGAGTACGGTAGAG GGTGGTGGAATTTCCTGTGTAGCGGTGAAATGCGTAGATATAGGAAGGAACACCAGTGGCGA AGGCGACCACCTGGACTGATACTGACACTGAGGTGCGAAAGCGTGGGGAGCAAACA

WCS417-V3V4	TGGGGAATATTGGACAATGGGCGAAAGCCTGATCCAGCCATGCCGCGTGTGTGAAGAAGGT CTTCGGATTGTAAAGCACTTTAAGTTGGGAGGAAGGGCAGTTACCTAATACGTGATTGTTTTGA CGTTACCGACAGAATAAGCACCGGCTAACTCTGTGCCAGCAGCCGCGGTAATACAGAGGGT GCAAGCGTTAATCGGAATTACTGGGCGTAAAGCGCGCGTAGGTGGTTTGTTAAGTTGGATGTG AAATCCCCGGGCTCAACCTGGGAACTGCATTCAAAACTGACTGACTAGAGTATGGTAGAGGG TGGTGGAATTTCCTGTGTAGCGGTGAAATGCGTAGATATAGGAAGGAACACCAGTGGCGAAG GCGACCACCTGGACTAATACTGACACTGAGGTGCGAAAGCGTGGGGAGCAAACA
CHA0-V3V4	TGGGGAATATTGGACAATGGGCGAAAGCCTGATCCAGCCATGCCGCGTGTGTGAAGAAGGT CTTCGGATTGTAAAGCACTTTAAGTTGGGAGGAAGGGCAGTTACCTAATACGTGATTGTTTTGA CGTTACCGACAGAATAAGCACCGGCTAACTCTGTGCCAGCAGCCGCGGTAATACAGAGGGT GCAAGCGTTAATCGGAATTACTGGGCGTAAAGCGCGCGTAGGTGGTTTGTTAAGTTGGATGTG AAAGCCCCGGGCTCAACCTGGGAACTGCATCCAAAACTGGCAAGCTAGAGTATGGTAGAGG GTGGTGGAATTTCCTGTGTAGCGGTGAAATGCGTAGATATAGGAAGGAACACCAGTGGCGAA GGCGACCACCTGGACTGATACTGACACTGAGGTGCGAAAGCGTGGGGAGCAAACA

Table S2. Sequences for the V3-V4 regions used as priors in the DADA2 pipeline. Related to STAR Methods.

Supplemental references

S1. Pieterse, C.M.J., Berendsen, R.L., de Jonge, R., Stringlis, I.A., Van Dijken, A.J.H., Van Pelt, J.A., Van Wees, S.C.M., Yu, K., Zamioudis, C., and Bakker, P.A.H.M. (2021). *Pseudomonas simiae* WCS417: star track of a model beneficial rhizobacterium. Plant Soil *461*, 245–263. 10.1007/s11104-020-04786-9.

S2. Stutz, Emil W., Défago, Geneviève, and Kern, Heinz (1986). Naturally occurring fluorescent pseudomonads involved in suppression of black root-rot of tobacco. American Phytopathological Society *76(2)*, 181–185. https://doi.org/10.1094/Phyto-76-181.

S3. Berendsen, R.L., van Verk, M.C., Stringlis, I.A., Zamioudis, C., Tommassen, J., Pieterse, C.M.J., and Bakker, P.A.H.M. (2015). Unearthing the genomes of plant-beneficial *Pseudomonas* model strains WCS358, WCS374 and WCS417. BMC Genomics *16*, 539. 10.1186/s12864-015-1632-z.

S4. de Boer, M., van der Sluis, I., van Loon, L.C., and Bakker, P.A.H.M. (1999). Combining fluorescent *Pseudomonas* spp. strains to enhance suppression of *Fusarium* wilt of radish. European Journal of Plant Pathology *105*, 201–210. 10.1023/A:1008761729073.

S5. de Weger, L.A., van Boxtel, R., van der Burg, B., Gruters, R.A., Geels, F.P., Schippers, B., and Lugtenberg, B. (1986). Siderophores and outer membrane proteins of antagonistic, plant-growth-stimulating, root-colonizing *Pseudomonas* spp. J Bacteriol *165*, 585–594. 10.1128/jb.165.2.585-594.1986.